

TOPICAL REVIEW

Coupled channels description of the α -decay fine structure

To cite this article: D S Delion *et al* 2018 *J. Phys. G: Nucl. Part. Phys.* **45** 053001

View the [article online](#) for updates and enhancements.

Topical Review

Coupled channels description of the α -decay fine structure

D S Delion^{1,2,3,6} , Zhongzhou Ren^{4,6}, A Dumitrescu^{1,2} and Dongdong Ni⁵

¹ ‘Horia Hulubei’ National Institute of Physics and Nuclear Engineering, 30 Reactorului, POB MG-6, Bucharest-Măgurele, RO-077125, România

² Academy of Romanian Scientists, 54 Splaiul Independenței, Bucharest, RO-050094, România

³ Bioterra University, 81 Gârlei str., Bucharest, RO-013724, România

⁴ School of Physics Science and Engineering, Tongji University, Shanghai 200092, People’s Republic of China

⁵ Space Science Institute, Macao University of Science and Technology, Macao, People’s Republic of China

E-mail: delion@theory.nipne.ro and zren@tongji.edu.cn

Received 27 November 2017, revised 16 January 2018

Accepted for publication 1 February 2018

Published 16 March 2018



CrossMark

Abstract

We review the coupled channels approach of α transitions to excited states. The α -decaying states are identified as narrow outgoing Gamow resonances in an α -daughter potential. The real part of the eigenvalue corresponds to the Q -value, while the imaginary part determines the half of the total α -decay width. We first review the calculations describing transitions to rotational states treated by the rigid rotator model, in even–even, odd-mass and odd–odd nuclei. It is found that the semiclassical method overestimates the branching ratios to excited 4^+ for some even–even α -emitters and fails in explaining the unexpected inversion of branching ratios of some odd-mass nuclei, while the coupled-channels results show good agreement with the experimental data. Then, we review the coupled channels method for α -transitions to 2^+ vibrational and transitional states. We present the results of the Coherent State Model that describes in a unified way the spectra of vibrational, transitional and rotational nuclei. We evidence general features of the α -decay fine structure, namely the linear dependence between α -intensities and excitation energy, the linear correlation between the strength of the α -core interaction and spectroscopic factor, and the inverse correlation between the nuclear collectivity, given by electromagnetic transitions, and α -clustering.

⁶ Author to whom any correspondence should be addressed.

Keywords: coupled channels method, fine structure of alpha-transitions, double folding potential, rotational–vibrational model, coherent state model

(Some figures may appear in colour only in the online journal)

1. Introduction

The simplest phenomenological description of α -decay half-lives uses the picture of a pre-formed α -cluster penetrating through the Coulomb barrier, proposed in 1928 by [1, 2]. This picture is based on the fact that the α -particle is the most bound nuclear system and for this reason it is widely accepted that it is born with some probability on the nuclear surface, where the nuclear density has a smaller value. A more sophisticated R -matrix theory calculates this probability, called spectroscopic factor, in terms of single particle proton plus neutron orbitals [3–7]. The α -transitions to excited states are very sensitive to nuclear structure details. They are used as an important tool to investigate the structure of low-lying states [8]. Along with the development of experimental facilities and the enhancement of experimental sensitivities, α -decay spectra have been measured with improved accuracy. Many deformed α emitters show a line spectrum of α groups corresponding to α -transitions to different daughter states, which is confirmed by the fact that the energy differences between various α groups fit with γ rays [9, 10]. This phenomenon is called the α -decay fine structure (with short-range α particles). It was first discovered by Rosenblum in 1929 [11]. Since then, the field of experiments that probe these α -transitions and their connection to the structure of the parent nuclei has flourished. For example, [12–28] deal mainly with the α -spectroscopy of medium-mass nuclei, with particular interest to the region around the $Z = 82$ shell closure. Experimental investigations of the α -emitters in the actinides region can be consulted in [29–38].

Attempts to explain the fine structure of the α -emission spectrum have been made soon after its discovery. In one of these attempts, Rasmussen and Segall performed the first numerical calculations of the α -decay fine structure by solving a set of coupled differential equations in 1956 [39]. In the last decade, the new challenge in α -decay studies is to interpret the α -decay fine structure observed in heavy deformed nuclei. The logic of theoretical investigations followed a path from semiclassical to coupled-channel calculations and from even–even, to odd-mass, and then to odd–odd nuclei. In addition, it should be particularly noted that sufficient knowledge of the α -decay fine structure in heavy nuclei is also helpful for future researches on superheavy nuclei [40–45], because α -decay in the superheavy mass region presents a powerful and precise tool to probe nuclear structure properties.

The α -transitions to the excited-state rotational band occur in vibrational or transitional nuclei and the branching ratio (b.r.) is quite low [46, 47]. The α -decay fine structure is clear-cut in even–even nuclei, generally from ground states (g.s.) 0^+ of parent nuclei to the low-lying members of g.s. rotational bands in daughter nuclei (i.e., 0^+ , 2^+ , 4^+ , 6^+ , ...). Furthermore, each member of the rotational band exhibits one single channel and the b.r. shows a clear decrease as one proceeds to the higher-lying members of the band. The situation for the case of odd- A and odd–odd emitters is much more complicated owing to unpaired nucleons. There are various rotational bands built on s.p. states or two-quasiparticle states. Also, the structure of parent states is generally different from that of the g.s. rotational band in daughter nuclei. The α -decay fine structure depends on both the structure differences between parent and daughter states and the decay energy of α -transitions. The structure differences accompany the decay with an additional centrifugal barrier. More importantly, they bring in some hindrances to the α -cluster formation. In general, the smaller the structure difference between

the parent and daughter states, the larger the probability of an α -transition between them. On the other hand, the final daughter states exhibit different excitation energies, which correspond to different decay energies. As one would expect, the larger the decay energy, the larger the probability of the corresponding α -transition. The interplay between these two aspects results in a line spectrum of α groups.

The main aim of this review is to present methods and results concerning the description of α -transitions to excited states in even–even and odd-mass nuclei in terms of the coupled channels formalism, by using various nuclear structure models.

2. General formalism

2.1. Equations

As already we mentioned, it is widely accepted that the α -particle is born on the nuclear surface, where the nuclear density has a smaller value, with some probability called spectroscopic factor [8]. Starting from this region it moves in the resulting nuclear plus Coulomb field of the daughter nucleus. The most general α -decay transition can be written

$$P(I_P) \rightarrow D(I) + \alpha(\ell), \quad (2.1)$$

in terms of

I_P denoting the spin/parity of the initial state in the parent nucleus (P),

I the spin/parity of the final state in the daughter nucleus (D) and

ℓ the angular momentum of the emitted α -particle.

The wave function of the system can be written as a multipole expansion [8] with the total spin of the initial state

$$\Psi_{I_P M_P}(\xi_D, \mathbf{R}) = \sum_{c=(I,\ell)} \frac{f_c(R)}{R} \mathcal{Y}_{I_P M_P}^{(c)}(\xi_D, \hat{R}). \quad (2.2)$$

The radial function $f_c(R)$ describes the α -daughter radial motion, where the index c denotes the emission channel $c \equiv (I, \ell)$. The ‘clustered’ ansatz of the wave function is expressed by the core-angular harmonics

$$\mathcal{Y}_{I_P M_P}^{(c)}(\xi_D, \hat{R}) = [\Phi_I(\xi_D) \otimes Y_\ell(\hat{R})]_{I_P M_P}, \quad (2.3)$$

where the symbol \otimes denotes the standard angular momentum coupling between the daughter (core) internal wave function $\Phi_{IM}(\xi_D)$, depending on the daughter degrees of freedom ξ_D , and the standard spherical harmonic $Y_{\ell m}(\hat{R})$, describing the relative angular motion of the α -daughter system. These core-angular harmonics satisfy the orthonormality condition

$$\langle \mathcal{Y}_{I_P M_P}^{(c)} | \mathcal{Y}_{I_P M_P}^{(c')} \rangle = \delta_{cc'}. \quad (2.4)$$

The α -daughter dynamics is described by the stationary Schrödinger equation

$$H \Psi_{I_P M_P}(\xi_D, \mathbf{R}) = Q_\alpha \Psi_{I_P M_P}(\xi_D, \mathbf{R}), \quad (2.5)$$

where Q_α is relative energy of the emitted α -particle, called the Q -value of the decay process. Due to the fact that all measured decay widths are by many orders of magnitude smaller than the corresponding Q -values, the stationarity approximation is a very good assumption. Hence, an α -decaying state is identified with a narrow resonant solution that contains only outgoing components. The Hamiltonian

$$H = -\frac{\hbar^2}{2\mu}\nabla_R^2 + H_D(\xi_D) + V(\xi_D, \mathbf{R}), \quad (2.6)$$

contains the kinetic operator, depending on the reduced mass $\mu = m_N 4A_D / (4 + A_D)$, a term describing the dynamics of the nuclear core $H_D(\xi_D)$

$$H_D \Phi_{IM_i}(\xi_D) = E_c \Phi_{IM_i}(\xi_D), \quad (2.7)$$

and the α -core interaction, which we split into spherical and deformed parts

$$V(\xi_D, \mathbf{R}) = V_0(\xi_D, R) + V_d(\xi_D, \mathbf{R}). \quad (2.8)$$

By using the orthonormality of the core-angular harmonics (2.4) in the superposition (2.2), one obtains in a standard way the coupled system of differential equations for radial components [8]

$$\frac{d^2 f_c(R)}{d\rho_c^2} = \sum_{c'} A_{cc'}(R) f_{c'}(R), \quad (2.9)$$

where the coupling matrix is given by

$$A_{cc'}(R) = \left[\frac{\ell(\ell+1)}{\rho_c^2} + \frac{V_0(\xi_D, R)}{Q_\alpha - E_c} - 1 \right] \delta_{cc'} + \frac{\langle \mathcal{Y}_{I_p}^{(c)} | V_d(\xi_D, \mathbf{R}) | \mathcal{Y}_{I_p}^{(c')} \rangle}{Q_\alpha - E_c}, \quad (2.10)$$

in terms of the channel reduced radius

$$\rho_c = \kappa_c R, \quad \kappa_c = \sqrt{\frac{2\mu(Q_\alpha - E_c)}{\hbar^2}}. \quad (2.11)$$

Let us mention that at large distances, where the field becomes spherical ($V_d \rightarrow 0$) and purely Coulombian, the system of equations has a simple form

$$\left[-\frac{d^2}{d\rho_c^2} + \frac{\ell(\ell+1)}{\rho_c^2} + \frac{\chi_c}{\rho_c} - 1 \right] f_c(\chi_c, \rho_c) = 0. \quad (2.12)$$

The solution in each channel c has the following asymptotic expression

$$f_c(\chi_c, \rho_c) \rightarrow N_c H_\ell^{(+)}(\chi_c, \rho_c), \quad (2.13)$$

in terms of the outgoing Coulomb–Hankel spherical wave, depending on the Coulomb–Sommerfeld parameter

$$\chi_c = \frac{2Z_D Z_\alpha}{\hbar v_c} \sim \frac{2Z_D Z_\alpha}{\sqrt{Q_\alpha - E_c}}, \quad (2.14)$$

and reduced radius (2.11). By using the continuity equation one obtains the total decay width as a sum of partial widths [8]

$$\Gamma = \sum_c \Gamma_c = \sum_c \hbar v_c \lim_{R \rightarrow \infty} |f_c(R)|^2 = \sum_c \hbar v_c |N_c|^2, \quad (2.15)$$

in terms of the center of mass velocity at infinity for each α -daughter channel $v_c = \frac{\hbar \kappa_c}{\mu}$. Each partial width can be formally rewritten in a factorized form at some radius R

$$\Gamma_c = 2\gamma_c^2(R) P_c(R), \quad (2.16)$$

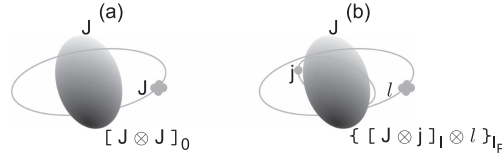


Figure 1. Panel (a) presents an even–even core coupled with an α particle to angular momentum $I_P = 0$. Panel (b) shows a core of angular momentum J coupled with an odd nucleon of spin j to angular momentum I , then coupled again with an α particle with angular momentum ℓ to total spin I_P .

in terms of the so-called reduced width and penetrability

$$\gamma_c^2(R) = \frac{\hbar^2}{2\mu R} |f_c(R)|^2$$

$$P_c(R) = \frac{\rho_c}{|H_\ell^{(+)}(\chi_c, \rho_c)|^2} = \frac{\rho_c}{F_\ell^2(\chi_c, \rho_c) + G_\ell^2(\chi_c, \rho_c)} \approx \frac{\rho_c}{G_\ell^2(\chi_c, \rho_c)}. \quad (2.17)$$

Here $F_\ell(\chi_c, \rho_c)$ and $G_\ell(\chi_c, \rho_c)$ are the standard regular and irregular spherical Coulomb functions, depending on Coulomb parameter χ_c and reduced radius $\rho_c = \kappa_c R$ in the channel c . For a large Coulomb barrier with respect to the Q -value, as it is the case for the α -decay, the regular function practically vanishes inside the barrier. The product in equation (2.16) does not depend upon the radius, but this representation allows us to estimate the decay width by using the wave function on the nuclear surface.

In the case of an initial even–even emitter in the ground state the initial spin $I_P = 0$ and therefore the α -particle rotates in the opposite direction with respect the daughter motion with $J = \ell$, as it is depicted in figure 1(a). The core-angular harmonics are given by $\mathcal{Y}_0^{(c)}(\xi_D, \hat{R})$, with $c = J$. For transitions from odd-mass nuclei, if the state of the unpaired nucleon remains unchanged during the decay process, then the transition is known as favored. Otherwise, it is called unfavored.

In the case of an odd-mass daughter nucleus its spin I is given by the coupling between the spin of the even–even core J and the single particle (s.p.) spin j . The wave function of the daughter nucleus is given by a particle-core ansatz

$$\Phi_{IM}(\xi_D, \mathbf{r}) = \sum_J X_I^{(J,j)} [\varphi_J(\xi_D) \otimes \psi_j(\mathbf{r})]_{IM}, \quad (2.18)$$

where $\varphi_J(\xi_D)$ is the wave function of the even–even core and $\psi_{jm}(\mathbf{r})$ are s.p. orbitals. The mixing coefficients are found by diagonalizing a quadrupole–quadrupole (QQ) interaction between the even–even core and the odd particle. A more general ansatz assumes a quasiparticle-core coupling. In odd–odd nuclei, the s.p. orbital is replaced by a proton–neutron wave function. The spin of the emitted α -particle has several values $|I_P - I| \leq \ell \leq I_P + I$. This situation is schematically shown in the panel (b) of the same figure.

2.2. Interaction

The analysis of the α -daughter interaction is a central issue of this field. One of the most popular methods is that of the double folding procedure, presented in [48–50]. The double folding potential that describes the elastic scattering of α -particles was extended to nuclei of medium mass number $A \sim 50$ –120 nuclei at energies from ~ 13 to 50 MeV in [51]. In [52], the experimental scattering data of nuclei with $A \sim 90$ –150 were systematically fitted at

energies around the Coulomb barrier. Thus, local potential parameter sets were obtained, having a real folding potential and an imaginary potential of a Woods–Saxon surface type.

The double folding procedure to estimate the α -core potential is given by the following integral [53–55]

$$V(\Omega_D, \mathbf{R}) = \int d\mathbf{r}_D \int d\mathbf{r}_\alpha \rho_D(\mathbf{r}_D) \rho_\alpha(\mathbf{r}_\alpha) v(\mathbf{R} + \mathbf{r}_D - \mathbf{r}_\alpha), \quad (2.19)$$

where v denotes the nucleon–nucleon force and ρ_X the nuclear densities of the daughter nucleus ($X = D$) and α -particle ($X = \alpha$). This method found much use in computing the potential between heavy ions having a Woods–Saxon shape for their densities. In our case, the density of the daughter nucleus is given by the aforementioned distribution, while the one of the α -particle is a Gaussian with standard parameters [49]. The resulting potential can be decomposed into a spherical (V_0) and a deformed part (V_d) as in equation (2.8). We suppose that the daughter nucleus has an axially deformed shape. A multipole expansion of the nuclear densities allows one to obtain the deformed part of the interaction

$$V_d(\Omega_D, \mathbf{R}) = \sum_{\lambda > 0} V_\lambda(R) \mathcal{Y}_\lambda(\Omega_D, \Omega), \quad (2.20)$$

where the angular component has the following ansatz

$$\mathcal{Y}_\lambda(\Omega_D, \Omega) = [Y_\lambda(\Omega_D) \otimes Y_\lambda(\Omega)]_0, \quad (2.21)$$

depending on the angle between the emitted α -particle and daughter nucleus Ω , as well as the angle determining the orientation of the nuclear symmetry axis Ω_D . Here, we replaced the standard by a shorthand notation $\mathcal{Y}_0^\lambda \rightarrow \mathcal{Y}_\lambda$. The multipole formfactors $V_\lambda(R)$ are given in terms of density distributions [55]. Some authors postulate the radial formfactors in a phenomenological way. The widely used potential is given by the M3Y nucleon–nucleon interaction with Reid soft core parametrisation [53–55] (see [8] for computational details). The resulting α -core potential has a Woods–Saxon shape and it is suitable for the treatment of α -transitions from well deformed nuclei, which are successfully described by the rigid rotor model. The decaying state is a resonant state in this potential, chosen by considering the so-called Wildermuth orthogonality condition simulating Pauli principle described in section 5 [56–58]. It is also possible to consider an alternative approach by using a monopole pocket-like shape [59, 60]

$$\begin{aligned} V_0(R) &= v_a \bar{V}_0(R), \quad R > R_m \\ &= c(R - R_{\min})^2 - v_0, \quad R \leq R_m, \end{aligned} \quad (2.22)$$

where \bar{V}_0 is the $\lambda = 0$ part of the Coulomb plus nuclear potential which is estimated by means of the double folding procedure. The parameters of the nuclear interaction between the α -particle and daughter nucleus defining \bar{V}_0 are determined from scattering experiments which assume that the α -particle exists with certainty, that is $v_a = 1$. Therefore, the interaction must be multiplied by a factor $v_a < 1$, thus simulating the formation of the cluster on the nuclear surface. The correct value of v_a is determined by the absolute value of the total decay width [60]. α -decay b.r. to members of the ground band have a weak dependence of this factor [59]. Another approach consists of leaving the interaction potential unquenched and taking into consideration the spectroscopic factor (2.32) as a measure of the particle formation probability, as in [61]. The second line of equation (2.22) is the repulsive core simulating the Pauli principle, namely the fact that the α -particle can exist only on the nuclear surface [62]. This core also fixes the energy of the first resonant state to the experimental Q -value Q_α [6, 59]. The total half-life and the partial decay widths do not depend upon the shape of this repulsive potential [59]. In [59], the procedure to determine the matching radius R_m and the

coordinate R_{\min} , corresponding to the minimal value v_0 , is described. It makes use of the equality between the external attractive potential and internal repulsion, up to their first derivative. This implies that the above interaction is continuous and dependent only on the potential depth v_0 . The deformed part of the potential (2.8) is given by equation (2.20) for rotational nuclei and by a QQ interaction for vibrational emitters

$$V_d(\xi_D, \mathbf{R}) = -C_0(R - R_{\min}) \frac{dV_0(R)}{dR} \sqrt{5} [Q_2(\xi_D) \otimes Y_2(\Omega)]_0, \quad (2.23)$$

where $Q_2(\xi_D)$ is the quadrupole operator corresponding to the daughter nucleus, and $Y_2(\Omega)$ represents the emitted α -particle. Let us mention that this type of QQ interaction can be used as a general ansatz within a more general Coherent State Model (CSM), describing low-lying vibrational, transitional and rotational spectra.

2.3. Resonances

A state which decays by α -emission is identified with a narrow resonant solution of the system of equations (2.9) that contains only outgoing components. The first step required in order to solve this system of equations is to define the internal and external fundamental solutions which satisfy the boundary conditions

$$\begin{aligned} \mathcal{R}_{cn}(R) &\xrightarrow{R \rightarrow 0} \delta_{cn} \varepsilon_c, \\ \mathcal{H}_{cn}^{(+)}(R) &\equiv \mathcal{G}_{cn}(R) + i\mathcal{F}_{cn}(R) \xrightarrow{R \rightarrow \infty} \delta_{cn} H_c^{+}(\kappa_c R) \\ &\equiv \delta_{cn} [G_\ell(\kappa_c R) + iF_\ell(\kappa_c R)], \end{aligned} \quad (2.24)$$

where ε_c are arbitrary small numbers. Here, the index c labels the component while n indexes the solution. A superposition of N fundamental solutions builds each component of the final solution. Imposing the matching conditions at a radius R_1 inside the barrier, one obtains

$$\begin{aligned} f_c(R_1) &= \sum_n \mathcal{R}_{cn}(R_1) M_n = \sum_n \mathcal{H}_{cn}^{+}(R_1) N_n \\ \frac{df_c(R_1)}{dR} &= \sum_n \frac{d\mathcal{R}_{cn}(R_1)}{dR} M_n = \sum_n \frac{d\mathcal{H}_{cn}^{+}(R_1)}{dR} N_n, \end{aligned} \quad (2.25)$$

where the quantities N_n are called scattering amplitudes. One thus finds the following secular equation

$$\begin{vmatrix} \mathcal{R}(R_1) & \mathcal{H}^{+}(R_1) \\ \frac{d\mathcal{R}(R_1)}{dR} & \frac{d\mathcal{H}^{+}(R_1)}{dR} \end{vmatrix} \approx \begin{vmatrix} \mathcal{R}(R_1) & \mathcal{G}(R_1) \\ \frac{d\mathcal{R}(R_1)}{dR} & \frac{d\mathcal{G}(R_1)}{dR} \end{vmatrix} = 0. \quad (2.26)$$

The first condition is fulfilled for the complex energies of the resonant states. They practically coincide with the real scattering resonant states, due to the fact that the imaginary parts of energies are much smaller than the corresponding real parts, which implies vanishing regular Coulomb functions F_ℓ inside the barrier. The roots of the equation (2.26) do not depend upon the matching radius R_1 , due to the fact that both internal and external solutions satisfy the same Schrödinger equation. To obtain the unknown coefficients M_n and N_n , it is required to normalize the wave function in the internal region

$$\sum_c \int_0^{R_2} |f_c(R)|^2 dR = 1, \quad (2.27)$$

where R_2 is the external turning point.

2.4. Observables

We will determine the α -decay fine structure by calculating the logarithm of the ratio between decay widths to ground $c = 0$ ($E_c = 0$) and excited states c , i.e.

$$\mathcal{J}_c \equiv \log_{10} \frac{\Gamma_0}{\Gamma_c}. \quad (2.28)$$

We call the quantity \mathcal{J}_c the intensity of the α -decay to the c th state [59]. The total half-life is related to the decay width through the formula

$$T = \frac{\hbar \ln 2}{\Gamma}. \quad (2.29)$$

α -transitions to excited states can be better analyzed by extracting the influence of the Coulomb barrier in terms of the hindrance factor (HF), defined by the ratio between formation probabilities to ground and excited states (as defined in [63]). By using the representation (2.16) of the decay width in terms of the reduced width and penetrability, the logarithm of the this quantity can be written as follows

$$\log_{10} \text{HF}_c \equiv \log_{10} \frac{\gamma_0^2}{\gamma_c^2} = \mathcal{J}_c - \log_{10} \frac{P_0}{P_c}. \quad (2.30)$$

where the reduced width (or preformation probability) is computed at the touching radius

$$R = 1.2(4^{1/3} + A_D^{1/3}), \quad (2.31)$$

in terms of the mass number of the daughter nucleus A_D .

The α -particle formation probability is given by the spectroscopic factor

$$S = \frac{\Gamma_{\text{exp}}}{\Gamma_{\text{th}}} = \frac{T_{\text{th}}}{T_{\text{exp}}}, \quad (2.32)$$

which is less than unity. One also defines the spectroscopic factor for each channel c

$$S_c = \frac{\Gamma_0^{\text{exp}}}{\Gamma_c^{\text{th}}}. \quad (2.33)$$

Let us mention here that the spectroscopic factor can be estimated microscopically as the integral of the preformation amplitude squared, defined as the antisymmetrised overlap between parent and daughter times the relative α -particle wave functions [8]

$$S_c^{(\text{micr})} = \int_0^\infty |\mathcal{A} \langle \Psi^P | \Psi_c^D \Psi^\alpha \rangle|^2 dR. \quad (2.34)$$

Finally one can introduce the so-called suppression factor (SF) that is very useful when analyzing the adequacy of a theory, through the formula:

$$\log_{10} \text{SF}_c = \mathcal{J}_c^{\text{exp}} - \mathcal{J}_c^{\text{th}}. \quad (2.35)$$

2.5. Systematics

By using the analytic semiclassical representation of the Coulomb function [8] one obtains a linear dependence between the logarithm of the penetrability and the Coulomb parameter

$$\log_{10} P_c \sim \chi_c = \frac{4Z_D}{\hbar v_c} \sim \frac{Z_D}{\sqrt{Q_\alpha - E_c}}. \quad (2.36)$$

On the other hand, by fitting the realistic pocket-like potential (2.22) to a shifted harmonic oscillator with frequency ω that is matched to the Coulomb barrier at the radius R_B , one obtains the so-called universal law for reduced widths [62]

$$\log_{10} \gamma_c^2(R_B) = -\frac{\log_{10} \mathbf{e}^2}{\hbar\omega} V_{\text{frag}} + \log_{10} \frac{\hbar^2 \mathcal{A}_c^2}{2\mathbf{e}\mu R_B}, \quad (2.37)$$

in terms of the fragmentation potential

$$V_{\text{frag}} = V_C - (Q_\alpha - E_c), \quad V_C = \frac{2Z_D e^2}{R_B}. \quad (2.38)$$

Here $\mathbf{e} \approx 2.71828$, $e^2 = 1.44 \text{ MeV fm}$ and \mathcal{A}_c is the channel amplitude of the α -particle wave function peaked on the nuclear surface. This law together with (2.36) has the following consequences:

- (1) The Viola-Seaborg rule for the partial half-lives [64]

$$\log_{10} T_c = \frac{aZ_D + b}{\sqrt{Q_\alpha - E_c}} + cZ_D + d \equiv V_c; \quad (2.39)$$

- (2) The logarithm of the HF becomes proportional to the excitation energy of the daughter nucleus [8]

$$\begin{aligned} \log_{10} \text{HF}_c &= \frac{\log_{10} \mathbf{e}^2}{\hbar\omega} E_c + \log_{10} \frac{\mathcal{A}_0^2}{\mathcal{A}_c^2} \\ &\equiv e_c E_c + f_c; \end{aligned} \quad (2.40)$$

- (3) By using equation (2.30) one obtains a similar rule for intensities

$$\mathcal{J}_c = g_c E_c + h_c. \quad (2.41)$$

Experimentally measured α -transitions were recently reviewed in [65] by using the ENSDF database maintained by BNL [46]. A well-known systematics for α -transitions between ground states is given by the Viola-Seaborg rule (2.39), where the logarithm of the total half-life depends on the Coulomb parameter and charge number of the daughter nucleus. It was useful in describing transitions between ground states in the case of α -decay [66], as well as proton [67] and heavy-cluster emission [68, 69].

Other simple formulas for α -emission have been provided in [70, 71]. Because the channel Coulomb parameter (2.14) is a function of the excitation energy of the daughter nucleus, this rule was generalized for partial half-lives of transitions to excited states by equation (2.39), written in terms of the channel daughter spin $c = I$. The generalized version of the Viola-Seaborg rule is very well satisfied by all available experimental data concerning transitions to excited states with $1 \leq I \leq 6$, as can be seen for even–even emitters in figure 2(a), as well as for odd-mass emitters in the cases of favored (b) and unfavored transitions (c) [65]. It is to be noticed that one obtains similar values of the parameters both for even–even and odd-mass emitters, in the situation of favored as well as unfavored transitions. We will analyze in our review the other rules for HF (2.40) and intensities (2.41).

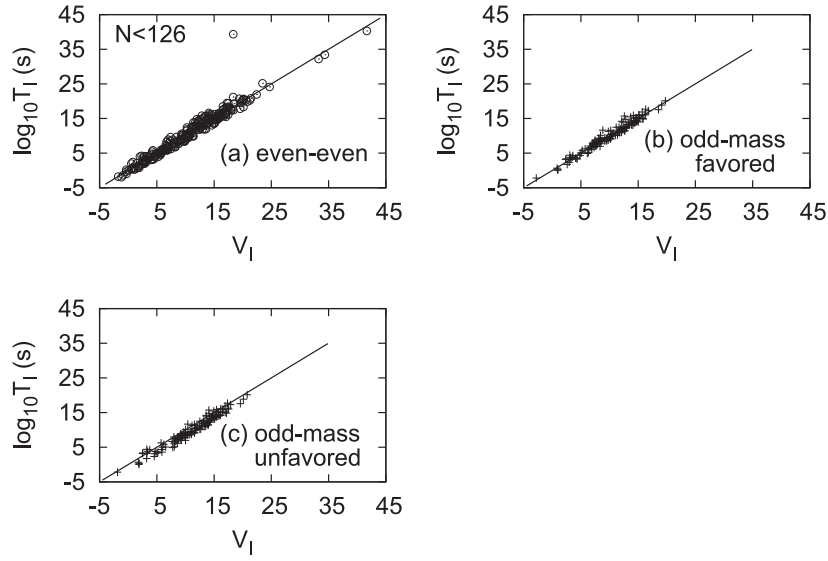


Figure 2. Logarithm of the partial half-life versus the generalized Viola-Seaborg parameter (2.39) for even–even (a), odd-mass favored (b) and odd-mass unfavored emitters (c). Here we considered data with $1 \leq I \leq 6$ in daughter nuclei. The parameters of the fitting lines defined by equation (2.39) are given in [65]. Adapted figure with permission from [65], Copyright (2015) by the American Physical Society.

3. Semiclassical approach

The semiclassical calculations for α -decay can be divided in two categories. The first family is based on the preformed-cluster model of Blendowske and Walliser [72–79]. The decay width is evaluated as a product of three model-dependent quantities: the frequency of assault on the barrier per second ν , the cluster preformation probability on the nuclear surface P_α , and the barrier penetration probability of the (preformed) cluster P . The second family is based on the fission theory describing the decay process by a continuous change of geometrical shapes [80–84]. Note that the cluster is considered to be formed gradually during the adiabatic rearrangements of parent nuclei. The decay width is expressed as a product of two model-dependent quantities: the frequency of oscillations in the fission mode ν_f (or the zero point vibration energy $E_\nu = h\nu_f/2$) and the barrier penetration probability P . In both cases, the α -decay process is treated as a one-dimensional problem and the one-dimensional Wentzel–Kramers–Brillouin (WKB) semiclassical approximation is used to calculate the penetration probability P as follows,

$$P = \exp\left(-\frac{2}{\hbar} \int_{R_1}^{R_2} \sqrt{2\mu [V(R) - Q_\alpha]} dR\right), \quad (4.1)$$

where R_1 and R_2 are the inner and outer turning points satisfying the expression $V(R_1) = V(R_2) = Q_\alpha$. The semiclassical calculations have proved to be successful in reproducing the experimental α -decay half-lives especially for favored α -decay [74–84]. As a straightforward extension for the fine structure, one treats the decay channels involved as individual events with different decay energies and various centrifugal barriers together with WKB penetration probabilities that are separately evaluated for them [85–89]. This procedure has a serious drawback. That is, it does not address the question of coupling among various

decay channels. Nevertheless, it serves as a good attempt for the fine structure owing to practical conveniences. In 2006, Xu and Ren proposed the simple WKB barrier penetration approach (belonging to the first category) for the α -decay b.r. to excited states of even–even nuclei [85, 86]. The interaction potential $V(R)$ in equation (4.1) consists of the Coulomb and centrifugal potentials, $V(R) = Z_1 Z_2 e^2 / R + \ell(\ell + 1)\hbar^2 / (2\mu R^2)$, where Z_1 and Z_2 are, respectively, the atomic numbers of the α particle and the daughter nucleus, and μ is the reduced mass of the α -daughter system. In the standard square potential well, the inner turning point is approximated by the touching radius R_0 . At this radius the height of the centrifugal barrier is significantly smaller relative to the height of the Coulomb barrier,

$$\xi = \frac{\ell(\ell + 1)\hbar^2}{2\mu R_0^2} \bigg/ \frac{Z_c Z_d e^2}{R_0} \simeq 0.002\ell(\ell + 1). \quad (4.2)$$

By expansion in terms of the small quantity ξ , the penetration probability is given in a straightforward manner [10, 85],

$$P(Q_\alpha, E_c, \ell) = \exp(4\sqrt{2\mu Z_1 Z_2 e^2 R_0} / \hbar) \\ \times \exp(-Z_1 Z_2 e^2 \pi \sqrt{2\mu / (Q_\alpha - E_c)} / \hbar) \exp(-2\xi \sqrt{2\mu Z_1 Z_2 e^2 R_0} / \hbar). \quad (4.3)$$

The first term remains constant for one decay having no influence on the fine structure, the second term accounts for the influence of the excitation energy E_c on the penetration, and the third term accounts for the influence of the additional centrifugal barrier. The b.r. for the α -transitions to ground 0^+ and excited 2^+ states are reproduced with satisfying accuracy. However, a significant overestimation emerges for the branching ratios to excited 4^+ states in the α -decay of $^{224-230}\text{Th}$, $^{228-238}\text{U}$, $^{236-244}\text{Pu}$, $^{240-248}\text{Cm}$, $^{240-252}\text{Cf}$, and $^{250-254}\text{Fm}$. This was called the abnormality of excited 4^+ states [85].

In 2009, Denisov and Khudenko [87] further investigated α -decays to ground and excited states for heavy deformed nuclei in the unified model for α -decay and α -capture (UMADAC). This model also belongs to the first category. The calculated b.r. show good agreement with the experimental data for $\ell = 0$ and $\ell = 2$ transitions, corresponding to ground 0^+ and excited 2^+ states in daughter nuclei. But the abnormal overestimation still exists for the b.r. to excited 4^+ states. Then, the semiclassical calculations of the second category were extended to describe the fine structure as well. In 2010, the α -decays to the members 0^+ , 2^+ , and 4^+ of the g.s. rotational band were studied for even–even nuclei in the generalized liquid drop model [88]. As previously found, the α -decay intensities to 0^+ and 2^+ states are in good agreement with the experimental data while the α -decay intensities to 4^+ states are apparently overestimated for the α -decays of some Pu, Cm, and Fm isotopes. Santhosh *et al* also performed systematic calculations of the α -decay fine structure observed in even–even emitters within the Coulomb and proximity potential model for deformed nuclei (CPPMDN) [89]. There is still a considerable overestimation of the b.r. to excited 4^+ states for some Pu, Cm, and Cf emitters. In a word, the semiclassical calculations of both kinds tend to overestimate the b.r. to excited 4^+ states and microscopic calculations are required to describe them.

To gain clear insight into such an unwelcome overestimation, we take the α -decay fine structure observed in the decay chain $^{246}\text{Cf} \rightarrow ^{242}\text{Cm} \rightarrow ^{238}\text{Pu}$ for an example and list in table 1 the detailed results obtained from the various semiclassical calculations mentioned above. As can be seen, all the semiclassical models tend to overestimate the b.r. to excited 4^+ states by more than one order of magnitude except for the CPPMDN result for the emitter ^{238}Pu where the b.r. is underestimated by a factor of roughly 20.

Table 1. Branching ratio (b.r.) to five low-lying members of the g.s. rotational band in the α -decay chain of $^{246}\text{Cf} \rightarrow ^{242}\text{Cm} \rightarrow ^{238}\text{Pu}$. The b.r. is given as a percentage (in %). The comparison of the theoretical results with the experimental data is shown and the calculated results are divided into two groups, semiclassical and coupled-channel results.

Transition	b.r. (exp)	b.r. (semiclassical)				b.r. (coupled-channel)		
		[85]	[87]	[88]	[89]	[60]	[58]	[61]
$^{246}\text{Cf} \rightarrow 0^+$	79.3(10)	73.9	55.9	—	65.58	61.74	70.83	71.45
$\rightarrow 2^+$	20.6(10)	24.3	33.0	—	29.38	38.07	28.86	28.38
$\rightarrow 4^+$	0.15(2)	1.82	9.79	—	4.71	0.19	0.29	0.17
$\rightarrow 6^+$	≈ 0.016	0.032	1.35	—	0.270	—	0.0236	0.00235
$\rightarrow 8^+$	—	—	—	—	—	—	$1.47 \cdot 10^{-4}$	—
$^{242}\text{Cm} \rightarrow 0^+$	74.08(7)	76.0	59.0	70.91	68.87	63.30	68.87	82.75
$\rightarrow 2^+$	25.92(6)	22.7	32.3	26.47	28.00	36.60	31.04	17.21
$\rightarrow 4^+$	0.035(2)	1.333	7.85	2.62	3.58	0.101	0.077	0.040
$\rightarrow 6^+$	0.0046(5)	0.0152	0.82	—	0.149	—	0.0053	0.000334
$\rightarrow 8^+$	$2.0 \cdot 10^{-5}$	$3.2 \cdot 10^{-5}$	0.0345	—	0.00210	—	$3.79 \cdot 10^{-5}$	—
$^{238}\text{Pu} \rightarrow 0^+$	70.91(10)	77.41	62.00	72.75	70.72	64.96	67.63	69.85
$\rightarrow 2^+$	28.98(10)	21.52	31.20	25.17	29.32	34.97	32.02	29.93
$\rightarrow 4^+$	0.105(5)	1.06	6.28	2.08	0.00538	0.069	0.343	0.213
$\rightarrow 6^+$	0.0030(1)	0.009	0.492	—	0.000177	—	0.00049	$5.65 \cdot 10^{-5}$
$\rightarrow 8^+$	$6.8(4) \cdot 10^{-6}$	$1.41 \cdot 10^{-5}$	0.0144	—	$1.86 \cdot 10^{-6}$	—	$2.03 \cdot 10^{-5}$	—

The gross features of the α -decay fine structure were described within the semiclassical approach by Delion *et al* in [90], by using a realistic α -daughter double folding potential. The most relevant part of this potential is the region between the inner and outermost turning points, where it can very well be approximated by

$$\begin{aligned} V(R) &= c - a(R - R_0)^2, \quad R \leq R_m \\ &= 2Ze^2/R, \quad R > R_m. \end{aligned} \quad (4.4)$$

The parameters are found by a fitting procedure, while the matching radius R_m is determined by imposing the continuity of the potential. This method was applied to describe α -decay from even–even emitters to yrast states in the daughter nuclei for which there are available experimental data [91]. The partial decay widths were evaluated by using the spherical semiclassical approximation, which is known to be 1%–2% accurate with respect to the exact solution [8]. The action integral for the nuclear interaction using the expression of equation (4.4) can be evaluated analytically. It is found that $R_m \approx R_0 + 0.3$ fm.

The partial decay width to the excited state with spin I and excitation energy E_c is proportional to the exponent of the sum of the two action integrals [8],

$$\begin{aligned} \Gamma_c^{(\text{th})} &= \exp \left\{ -2 \left[K_{\text{int}} \left(Q_\alpha - E_c - \frac{\hbar^2 \ell(\ell + 1)}{2\mu \tilde{R}^2} \right) \right. \right. \\ &\quad \left. \left. + K_{\text{ext}}(\chi_c, \kappa_c R_0) + \frac{\ell(\ell + 1)}{\chi_c} \sqrt{\frac{\kappa_c R_0}{\chi_c} - 1} \right] \right\}, \end{aligned} \quad (4.5)$$

where the centrifugal potential was evaluated at

$$\tilde{R} = (R_1 + R_0)/2 = R_0 - \sqrt{c/a}/2. \quad (4.6)$$

The inner action integral is given by

$$\begin{aligned} K_{\text{int}}(Q_\alpha) &= \int_{R_1}^{R_0} \sqrt{\frac{2\mu}{\hbar^2} [-a(R - R_0)^2 + c - Q_\alpha]} dR \\ &= \frac{1}{2} \sqrt{\frac{2\mu}{\hbar^2}} (R_0 - R_1) \sqrt{-a(R_0 - R_1)^2 + c - Q_\alpha} \\ &\quad + \sqrt{\frac{2\mu}{\hbar^2}} \frac{(c - Q_\alpha)}{2\sqrt{a}} \tan^{-1} \left(\frac{\sqrt{a}(R_0 - R_1)}{\sqrt{-a(R_0 - R_1)^2 + c - Q_\alpha}} \right), \end{aligned} \quad (4.7)$$

where R_1 is the inner turning point $R_1 = R_0 - \sqrt{\frac{c - Q_\alpha}{a}}$. The outer part of the action integral is given by

$$K_{\text{ext}}(\chi_c, \rho_0) = \int_{\rho_0}^{\chi_c} \sqrt{\frac{\chi_c}{\rho} - 1} d\rho = \chi_c \left(\cos^{-1} \sqrt{\frac{\rho_0}{\chi_c}} - \sqrt{\frac{\rho_0}{\chi_c} - 1} \sqrt{\frac{\rho_0}{\chi_c}} \right). \quad (4.8)$$

In figure 3 were analyzed available experimental data concerning α -decays to excited states in even–even nuclei [61]. Here there are plotted the intensities defined by equation (2.28) versus the excitation energy E_2 of daughter nuclei corresponding to (a) $c = J = 2$, (b) $c = J = 4$ and (c) $c = J = 6$. In this figure, the experimental values are represented by dark symbols while open symbols correspond to the computed results. One sees that the experimental features are reasonably well reproduced by the theoretical estimates. One notices the linear increasing trend of the intensity \mathcal{I}_2 , as predicted in [62].

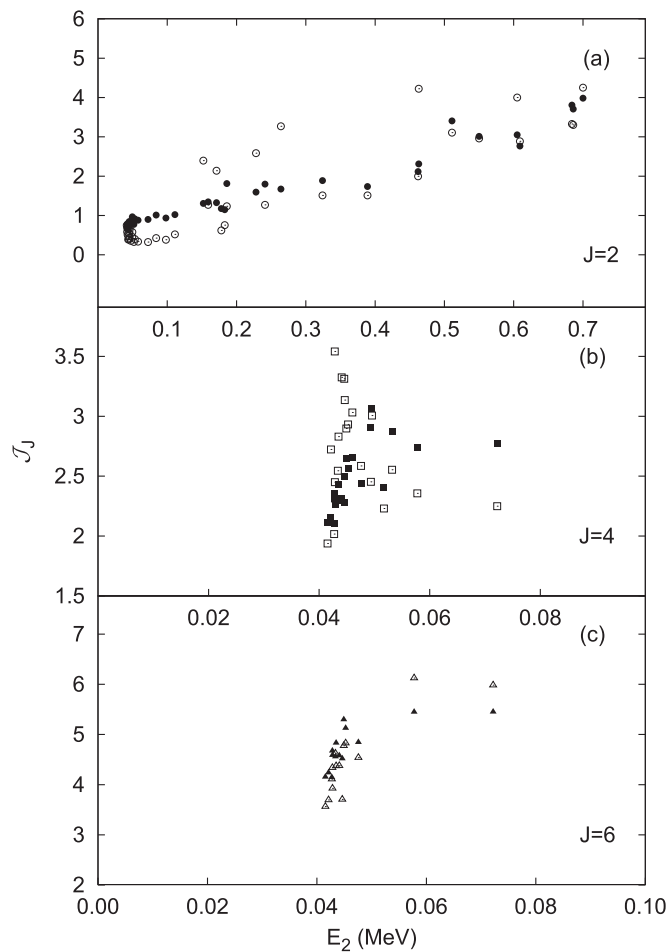


Figure 3. Intensity (2.28) versus the excitation energy E_2 of daughter nuclei for $c = J = 2$ (a) $c = J = 4$ (b) and $c = J = 6$ (c). The experimental values (adapted from [91]. © IOP Publishing Ltd. All rights reserved.) are represented by dark symbols while open symbols correspond to the theoretical estimates.

Finally, let us mention that the deformed WKB approach, called Fröman method [92], was used to estimate HF's in rotational nuclei by using a simple phenomenological ansatz for the preformation factor in [93].

4. Cluster-core model

A cluster model describes the α -particle dynamics by a spherical Schrödinger equation using an appropriate phenomenologic potential. Due to its simplicity it became very popular for various simple systematic calculations concerning transitions to ground and excited states. The α -transitions between ground states remain an interesting research topic, with recent results found in [94–96]. G.s. transitions were treated alongside exotic decay processes from heavy nuclei in [97], using a cluster model that employed a local, effective cluster-core potential based on a folding procedure. This model was extended in [98], so that it could take

into account the different sizes of the emitted fragments. This yielded a good reproduction of measured half-lives both for exotic and α -emission processes using a fixed set of parameters. Buck *et al* [99–102] have shown that the assumption of a preformed α -cluster in an orbit with a large global quantum number in heavy nuclei is very fruitful in explaining the observed partial half-lives for g.s. to g.s. transitions in even–even nuclei and favored transitions in odd-mass nuclei. In the even–even case, this procedure was also employed for exotic decays. A version of this model using a more realistic interaction potential was presented in [103]. Emphasis on the favored α -decay of odd-mass nuclei using a simple cluster model was put in [104]. α -clustering in ^{212}Po has been thoroughly investigated as well. In [105], the decay properties in the α and γ channels of the low-lying states of this isotope have been studied using an α -cluster model. The known lifetimes of the decaying states and the α branching ratios have been reproduced with a reasonable accuracy. In [106], a model describing an α -cluster in orbit around a closed shell with a universal interaction was used to give a description of the energy spectrum, $B(E2)$ transition strengths, α -decay widths and differential cross sections for the systems corresponding to an α -cluster interacting with a ^{16}O and ^{40}Ca core. In [107], the same procedure was extended to ^{212}Po and to the consistent description of favored α -decay half-lives throughout the Periodic table. The interaction thus developed was furthermore constrained in [108], where it was shown that a suitable parametrization could give an adequate description of the low-energy positive-parity structure properties of ^{212}Po as well as the differential cross sections for low-energy α -scattering on a ^{208}Pb target.

5. Rotational nuclei

Rotational even–even emitters are well deformed nuclei with a quasirotational spectrum starting with $E_{2+} < 100$ keV. The first calculations of the α -decay widths in rotational nuclei within the coupled channels approach were given in [39]. During last two decades a large amount of data became available in regard to the α -decay fine structure, as can be seen in [46, 91]. These data were analyzed within the coupled channels formalism [59, 60], by using the double folding potential plus a repulsive core simulating the Pauli principle. Also, the coupled channels analysis of the α -decay fine structure using the double folding potential together with the Wildermuth rule to simulate the Pauli principle was presented in several papers [56–58, 109, 110] and it will be analyzed in the next sub-section.

5.1. Double folding interaction plus repulsive core

Here we summarize the main results concerning α -transitions to rotational states given in [59, 60], by using a double folding α -core interaction plus a repulsive core to simulate the Pauli principle, namely the fact that the α -particle can be formed only on the nuclear surface, as described in section 2. Let us consider an α -decay process $P \rightarrow D(J) + \alpha$, where J denotes the spin of the rotational state of an even–even nucleus, i.e. $J = 0, 2, 4, 6, \dots$. We describe the α -core dynamics by using the stationary Schrödinger equation (2.5), where the core coordinates, describing the orientation of the daughter major axis in the laboratory system, are given by the Euler angles $\xi_D = \Omega_D = (\varphi_D, \theta_D, 0)$.

The Hamiltonian of the α -transitions in the laboratory system of coordinates is given by equation (2.6). The interaction between nuclei is estimated in terms of the double folding method (2.19), by using for the α -particle a Gaussian with standard parameters [49]. The resulting potential can be divided into a spherical (V_0) and a deformed component (V_d) (2.8), which can be expanded in multipoles as in equation (2.20), depending on angular harmonics

(2.21). To this potential we will also add a simple repulsive core in the monopole channel, depending upon one independent parameter, as shown by equation (2.22). The role of this potential is to simulate the Pauli principle and to adjust the energy of the system to the experimental Q -value. The total half-life and the partial decay widths practically do not depend upon the shape of this repulsive potential [59].

5.2. Results for even–even emitters

If the rotational states of the core belong to the ground band (with the intrinsic angular momentum projection $K = 0$) the daughter wave functions satisfy the following eigenvalue equations

$$H_D Y_{JM}(\Omega_D) = E_J Y_{JM}(\Omega_D), \quad (5.1)$$

i.e. they are the normalised Wigner functions with $K = 0$. The α -daughter wave function is given by

$$\Psi(\mathbf{R}, \Omega_D) = \frac{1}{R} \sum_J f_J(R) \mathcal{Y}_J(\Omega_D, \Omega), \quad (5.2)$$

where we denoted the α -core angular harmonic by

$$\mathcal{Y}_J(\Omega_D, \Omega) = [Y_J(\Omega_D) \otimes Y_J(\Omega)]_0. \quad (5.3)$$

Therefore the rotation of the core is compensated by the rotation of the α -particle in the opposite direction, while the channel is defined by the spin of the daughter nucleus $c = J$. Using the orthonormality of the angular functions that enter the superposition (5.2), one obtains in a standard way the coupled system of differential equations for radial components (2.9) where the coupling matrix is given by equation (2.10). The matrix element of the deformed part of interaction is given in terms of the Clebsch–Gordan coefficients as follows

$$\langle \mathcal{Y}_J | V_d(R) | \mathcal{Y}_{J'} \rangle = \sum_{\lambda > 0} V_\lambda(R) \sqrt{\frac{2J+1}{4\pi(2J'+1)}} [\langle J, 0; \lambda, 0 | J', 0 \rangle]^2. \quad (5.4)$$

The system of radial equations (2.9) acquires the asymptotic Coulombian form (2.12) beyond $R = R_c + 4 \text{ fm}$, where $R_c = 1.2(A_D^{1/3} + A_\alpha^{1/3})$, because the higher multipoles of the potential $\lambda \neq 0$ are centered around the nuclear surface, as can be seen in figure 4.

In [59] was performed an analysis of α -decays for 20 rotational nuclei with known ratios \mathcal{J}_2 and \mathcal{J}_4 , and one where \mathcal{J}_4 was only given as a limit. In the more recent [60], the analysis is extended to 52 nuclei. The experimental data, namely the excitation energies, total half-lives and Q -values, were taken from the compilation [91]. The intensities for $J = 2^+$, $J = 4^+$ states and total half-lives, with respective uncertainties, were compared with the ENSDF database. Only one of the half-lives, namely ^{240}Pu , slightly differs from the value of [91]. The deformation parameters were taken from the systematics in [111]. This data for daughter nuclei is presented in table 1 of [59]. For a more extended analysis, see [60].

In figure 5(a) are given the quadrupole (squares) and hexadecapole deformations (triangles), while in (b) the experimental values of the ratios \mathcal{J}_2 , \mathcal{J}_4 (squares) are shown.

In order to describe absolute half-lives, a linear function with a negative slope was used together with the following relation for the quenching factor entering equation (2.22): $v_a = 0.668 - 0.004(A - 208)$. The value of the repulsive strength was taken as $c = 100 \text{ MeV fm}^{-2}$. One sees that the agreement with experimental data for \mathcal{J}_2 is very good. Concerning \mathcal{J}_4 , a very good agreement was achieved only for the $Z = 90$ isotope chain. For the last $Z = 96$ and $Z = 98$ chains, the agreement is within a half-order of magnitude, while the central peak, around the $Z = 94$ chain, is not reproduced. The main trend of the

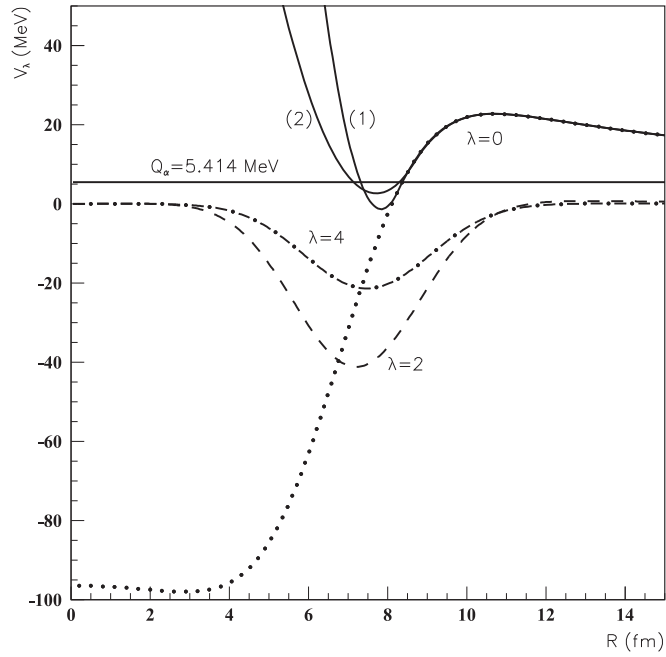


Figure 4. The radial components of the renormalised α -nucleus potential for $\lambda=0$ (dots), $\lambda=2$ (dashes) and $\lambda=4$ (dotted-dashed). The solid pocket-like curves (1) and (2) are the monopole parts of the interaction (2.22), giving the same Q -value. Their parameters are (1) $c = 90.117$ (MeV fm $^{-2}$), $Q_\alpha + v_0 = 10.272$ (MeV) and (2) $c = 30.296$ (MeV fm $^{-2}$), $Q_\alpha + v_0 = -3.816$ (MeV) [59]. The horizontal line denotes the Q -value. The dotted curve indicates the original double folding result. The decay process is $^{232}\text{Pu} \rightarrow ^{228}\text{U} + \alpha$. Adapted figure with permission from [59], Copyright (2006) by the American Physical Society.

experimental and computed \mathcal{J}_2 values in figure 5(b) is clearly correlated with the quadrupole deformation in (a). The same is true, but mainly for the computed \mathcal{J}_4 values, which are correlated with β_4 in (a). Thus, the existence of the central peak for experimental \mathcal{J}_4 data corresponding to the neutron chain $Z = 94$ seems to be out of the correlation between the fine structure and deformation parameters. However, the connection between decay widths and deformation parameters seems to be a universal property of emission processes. This feature was already evidenced for α -decays between ground states in [7].

5.3. Double folding interaction and the Wildermuth rule

In this picture, the original Woods–Saxon shape of the α -core potential given by the double folding procedure is kept, but the decaying state is chosen by considering the Wildermuth orthogonality condition [112]. The α -cluster is coupled to an axial-symmetric and well-deformed daughter nucleus. By expanding the total wave function of the system into a sum of partial waves one obtains the coupled-channel equations given by equations (2.9) and (2.10) for the radial wave function representing the relative motion of the α particle with respect to the daughter nucleus, $f_c(R)$. Here, $c \equiv (n\ell I)$ labels the channel quantum numbers, where n denotes the number of nodes, ℓ is the angular momentum carried by the emitted α particle and I is the spin of the parent

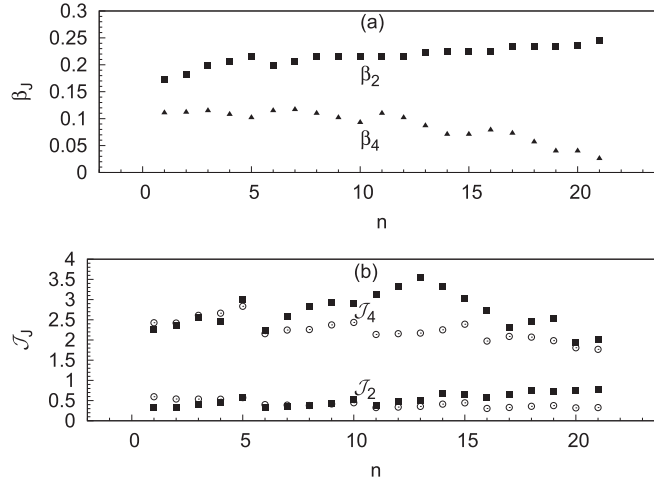


Figure 5. (a) Deformation parameters β_2 (squares) and β_4 (triangles) versus the decay number given by the first column in table 1 of [59], corresponding to $Z = 90$ ($n = 1 - 5$), $Z = 92$ ($n = 6 - 10$), $Z = 94$ ($n = 11 - 15$), $Z = 96$ ($n = 16 - 19$), $Z = 98$ ($n = 20 - 21$). (b) Experimental ratios \mathcal{J}_2 , \mathcal{J}_4 defined by equation (2.28) (squares) and the corresponding computed values (open circles). The attractive quenching parameter is given by the rule $v_a = 0.668 - 0.004(A - 208)$. The corresponding data in table 1 of [59] are labeled by the index (a). Adapted figure with permission from [59], Copyright (2006) by the American Physical Society.

nucleus. The angular momenta should satisfy the triangular relation owing to conservation of angular momentum, $|I_p - I| \leq \ell \leq |I_p + I|$. Thus, one shall consider many more decay channels in the α -emission from odd-mass or odd-odd nuclei than in the case of even-even nuclei, where (as noticed in the previous sub-section) α -decay occurs from ground $I_p = 0^+$ states of even-even nuclei and one obtains a single ℓ -value $\ell = J$ for the daughter state J .

To manipulate the dynamics, the key point is the interaction matrix $V_{cc'}(r)$ which contains most of the nuclear physics. The nuclear potential given by the double folding procedure with axially deformed density of the daughter nucleus provides a Woods-Saxon shape. It can be parametrized as follows

$$V_N(R, \theta) = \frac{V_0}{1 + \exp([R - R(\theta)]/a)}. \quad (5.5)$$

with the half-density radius $R(\theta) = r_0 A_D^{1/3} [1 + \beta_2 Y_{20}(\theta) + \beta_4 Y_{40}(\theta)]$, where θ is the orientation angle between the coordinate vector \mathbf{R} of the α -cluster and the symmetry axis of the core, and β_2 and β_4 are, respectively, quadrupole and hexadecapole deformation parameters of the deformed daughter nucleus. This potential not only has a simple and clear form but also achieves remarkable success in both nuclear structure and nuclear reactions. Moreover, it has practical advantages in numerical efficiency since the description of the fine structure requires high precision and good stability. There are two techniques available for the interaction matrix: one is the diagonalization of the coupling potential between channels [57, 113] and the other is the multipole expansion of the interaction potential [58, 114]. In the following, we shall present the theoretical basis of these two techniques, which are necessary to understand α -transitions from ground or isomeric states of the parent nucleus to various members of a rotational band in the daughter system.

In the diagonalization of the coupling potential between channels, one first treats the half-density radius $R(\theta)$ in the nuclear potential (5.5) as a dynamical operator [57, 113], $R(\theta) \rightarrow R_0 + \hat{O} = R_0 + R_D[\beta_2 Y_{20}(\theta) + \beta_4 Y_{40}(\theta)]$. Thus, the deformed nuclear potential is written as

$$V_N(R, \hat{O}) = \frac{V_0}{1 + \exp[(R - R_0 - \hat{O})/a]}. \quad (5.6)$$

In order to evaluate the matrix elements of the deformed potential between channel states $|I\rangle$ and $|I'\rangle$, one needs to search for the eigenvalues λ and eigenvectors $|\lambda\rangle$ of the operator \hat{O} , $\hat{O}|\lambda\rangle = \lambda|\lambda\rangle$. They can be easily obtained by diagonalizing the matrix \hat{O} , having the elements written in the channel representation as follows [57, 113]:

$$\hat{O}_{II'} = \sum_{\ell=2,4} \sqrt{\frac{(2\ell+1)(2I+1)}{4\pi(2I'+1)}} \beta_\ell R_D \langle I0; \ell 0 | I'0 \rangle^2. \quad (5.7)$$

Then, following the general methods one obtains the interaction matrix elements [57, 113]

$$V_{II'}^N(R) = \langle I | V_N(R, \hat{O}) | I' \rangle = \sum_{\lambda} \langle I | \lambda \rangle \langle \lambda | I' \rangle V_N(R, \lambda). \quad (5.8)$$

The multipole expansion of the nuclear potential V_N is given by (2.20) where only even values of λ appear in the summation owing to the axial symmetry. In the systematic calculations of α -decay half-lives, good convergence can be achieved by expanding the potential in spherical multipoles to the 4th order [56]. This is certainly not sufficient for the fine structure description because the numerical requirements increase greatly. The dependence of the theoretical results on the expansion order λ_{\max} is discussed. In general, the expansion order λ_{\max} has a value of more than 8, yielding the approximately same results. So it is sufficient to take $\lambda_{\max} = 10$ for proper convergence. Nevertheless, for the sake of good stability, the potential V_N is expanded in multipoles to order 12 in the calculations [58, 109, 110].

For rotational nuclei, the reduced matrix element of $Y_\lambda(\Omega)$ in equation (2.21), involving the daughter wave functions is given the standard expression in terms of the intrinsic angular momentum projection on the symmetry axis K [58, 114, 115]. If α -decay occurs from an even–even nucleus to the g.s. rotational band in the daughter nucleus, the intrinsic angular momentum projection K is equal to zero. In this way, the dynamic effects of the core nucleus are taken into full account in dealing with the interaction matrix element. It is then convenient to evaluate the coupling potential between channels $c = (\ell, I)$ and $c' = (\ell', I')$ [58, 114]:

$$V_{cc'}(R) = \sum_{\lambda} V_{\lambda}(R) \frac{(-1)^{\lambda}}{4\pi} (2\lambda+1) \sqrt{(2\ell'+1)(2I'+1)} \\ \times \langle \ell'0; \lambda 0 | \ell 0 \rangle \langle I'K; \lambda 0 | IK \rangle W(\ell' \lambda I; \ell I), \quad (5.9)$$

where $\langle a\alpha; b\beta | c\gamma \rangle$ is the Clebsch–Gordan coefficient and $W(abcd; ef)$ is the Racah coefficient.

After evaluating the interaction matrix elements, one can numerically integrate the coupled equations (2.9) with outgoing wave boundary conditions. The depth of the nuclear potential V_0 is adjusted to reproduce the experimental α -decay energies and the eigen-characteristic of the decay channels. The quantum numbers $(n\ell)$ of the solution are determined by the Wildermuth rule $G = 2n + \ell$ [112]. This rule is an approximate treatment of the Pauli exclusion principle, ensuring the α -cluster is completely outside of the shell occupied by the core nucleus. It also serves as a useful guide for setting the global quantum number G [116]. With the radial wave function $f_c(r)$, one can express the partial width of the channel c in the

form given by equation (2.15), i.e. [58, 114]

$$\Gamma_c(R) = \frac{\hbar^2 \kappa_c}{\mu} \frac{|f_c(R)|^2}{G_\ell^2(\kappa_c R) + F_\ell^2(\kappa_c R)}, \quad (5.10)$$

with $\kappa_c = \sqrt{2\mu(Q_\alpha - E_c)}/\hbar$. The above expression is valid only for large distances beyond the range of the nuclear potential and beyond the distance where the Coulomb potential can be regarded as spherically symmetric. Furthermore, the calculated results of Γ_c show rather weak sensitivity to the choice of R .

Then, one turns from the dynamics part of α -decay to the structure part. As is well known, the α -particle formation is a basic open problem for nuclear structure theory [117–119]. Although spin–orbit and Coulomb forces are strong in heavy nuclei, thereby suppressing cluster structure, there is evidence supporting an admixture of cluster states and mean-field states. A pure cluster configuration for ^{94}Mo and ^{212}Po was applied to investigate their g.s. bands, and the calculated $B(E2)$ values show good agreement with the experimental data [120]. The enhanced $E1$ transitions were observed for the first time in ^{212}Po and well interpreted by an α -clustering structure [121]. The α -preformation factor P_α is thus introduced for heavy nuclei, which measures the extent to which the α -cluster is formed on the nuclear surface. The microscopic evaluation probably offers the most rigorous treatment of P_α , but this approach is a formidably complex problem. Various shell models with improved ingredients have been devoted to this issue and the P_α factor was substantially underestimated by more than one order of magnitude [122, 123]. Varga *et al* [124] combined shell-model-type and cluster-model-type basis states to investigate the α -clustering component in ^{212}Po , and the α -decay width of ^{212}Po was well reproduced with the resulting P_α factor. But such calculations have not been extended for other heavy nuclei due to considerably increasing complication of the spatial configuration of nucleons. Experimentally, the α -preformation factor was extracted by (n, α) and (p, α) reaction analysis and by the analysis of α radioactivity of even–even nuclei [125]. It was found that the P_α factor has a value less than unity and varies smoothly in the open-shell region for heavy and superheavy nuclei [125]. In view of these difficulties and facts, one convenient way to fix the P_α value consists in taking the same preformation factor for a certain kind of nuclei (even–even, odd- A , and odd–odd) [56–58, 74, 75]. Very recently Xu *et al* have calculated the α -cluster formation in heavy nuclei by using the quartetting wave function approach [126]. It was found that the α -cluster formation is quite sensitive to the interplay of the mean field felt by the α -cluster and the Pauli blocking as a consequence of antisymmetrization.

The α -preformation factor P_α is of course important for absolute α -decay rates, but the detailed value of P_α has little influence on the α -decay fine structure since it is kept the same for various members of a rotational band in daughter nuclei. Considering that the internal structure of nuclear states has some influence on α -transitions as well, the hypothesis of Boltzmann distributions (BD) for daughter states was proposed $\rho(E_I) = \exp(-cE_I)$ [58, 109, 110], where E_I (in MeV) is the excitation energy of the daughter state I . Direct derivation of this hypothesis is rather difficult because it requires microscopic calculations of P_α , but there is indirect evidence supporting the validity of the hypothesis. Stewart *et al* [127] used the experimental b.r. to extract the internal amplitudes a_ℓ (associated with the α -preformation factor) for even–even actinide α -emitters. It was found that the calculated a_ℓ -values are essentially constant for all even–even actinide nuclei and they show the property $|a_0| > |a_2| > |a_4|$. Delion *et al* [62, 65] used a shifted harmonic oscillator plus Coulomb interaction to calculate the reduced width (proportional to the α -preformation factor) for even–even nuclei. It was shown that the reduced width to excited 2^+ states has an exponential

dependence on the excitation energy. In addition, one would like to emphasize that it is not the first time to propose the BD hypothesis in modern physics. As early as 1917, Einstein [128] had proposed the hypothesis of canonical distributions for molecules with a set of discrete states on the quantum theory of radiation. It is natural to generalize the canonical distribution from molecules to nuclei. These available theoretical works provide a sound basis for the BD hypothesis. Based on the experimental b.r. of even–even nuclei, the BD factor c is determined as $c = 2.38 \text{ MeV}^{-1}$ [58]. It is known that the low-lying excitation spectra of heavy nuclei exhibit energies from tens to hundreds of keV. So, the calculated b.r. to low-lying states show weak sensitivity to the BD factor c . Ultimately, the total width is given by $\Gamma = \sum_{\ell} P_{\alpha\rho}(E_I)\Gamma_{\ell}$ and the b.r. to the daughter state I is expressed as $\text{BR}_I = P_{\alpha\rho}(E_I)\sum_{\ell}\Gamma_{\ell}/\Gamma$.

5.4. Results for well-deformed even–even, odd–mass, and odd–odd emitters

In view of the fact that the α -decay spectra observed in well-deformed even–even nuclei are distinct (from ground 0^+ states to various members of the g.s. rotational band) and each member exhibits one single channel, the α -decay fine structures in even–even nuclei serve as a good test for the coupled-channels approach. First, the α -decays of even–even transfermium nuclei with $Z \geq 98$ were investigated in the coupled-channel representation [57], since they exhibit strong collective motion with a regular g.s. rotational spectrum. The diagonalization method was used to deal with the coupling potential and four channels were considered for one α -decay. The results shown in table 1 of [57] are in good agreement with the experimental data concerning both total α -decay half-lives and b.r. to various daughter states. As a rule, the most accurate results for the b.r. are those of the transitions to ground states and to excited 2^+ states. The results for the transitions to excited 4^+ states are less accurate. For the transitions to excited 6^+ states, the results are slightly worse but acceptable. Another approach, using the multipole expansion of the interaction, was also used to describe the α -decay fine structures in even–even nuclei [58]. Moreover, the dynamical effects of the core nucleus were introduced into the coupling potential and the BD hypothesis for nuclear states was adopted for daughter nuclei. Five-channels calculations were performed for the α -decay fine structures observed in 35 well-deformed even–even nuclei with $Z = 92 - 106$. The detailed results can be found in [58, 116]. The experimental b.r. to 0^+ , 2^+ , 4^+ , 6^+ , and 8^+ states are, respectively, reproduced with mean factors of 1.1, 1.3, 2.7, 3.3, and 3.2. In particular, the five-channels calculations give a precise description of the b.r. to excited 4^+ states in contrast to the semiclassical calculations overestimating them by more than one order of magnitude. In table 1, the coupled-channel results obtained from different models are also displayed for comparison. The comparison with the semiclassical results gives a strong indication of the importance of the coupling effects, which cannot be ignored especially for the transitions to highly excited states. For the b.r. to 0^+ , 2^+ , and 4^+ states, the five-channels results of [58] generally follow the theoretical results of [61] and all of them reproduce the experimental data well. The experimental b.r. to 6^+ states are quite small (less than 0.02%). It is hard to calculate such small components accurately and safely because they are rather sensitive to various aspects in a complicated system. As expected, the five-channels calculations of [58] and the four-channels calculations of [61] yield different results for them in some cases.

The fine structure observed in α -decay is closely associated with the structure properties of daughter nuclei. It is interesting to check the sensitivity of the theoretical results to the structure properties of daughter nuclei. As an example, we take the fine structure observed in the α -decay of ^{244}Cm . First, five-channels calculations are separately performed with different

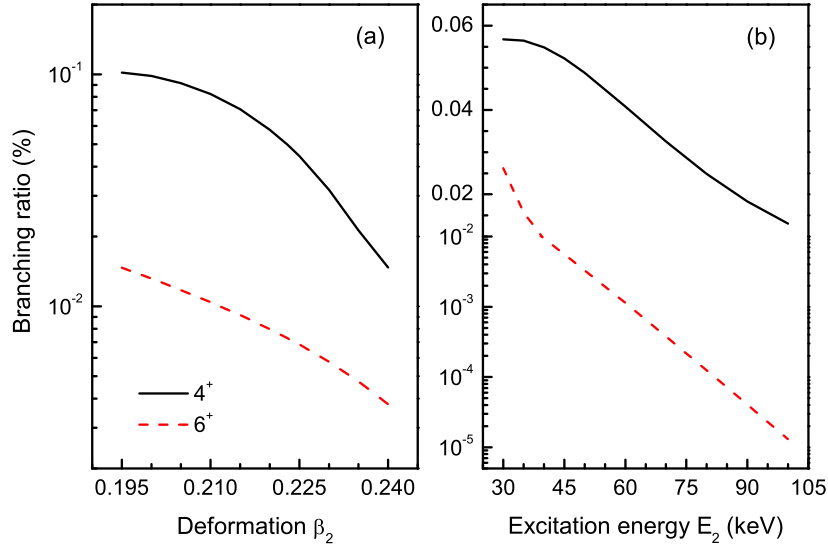


Figure 6. Dependence of the calculated branching ratios to excited 4⁺ and 6⁺ states upon the quadrupole deformation β_2 (a) and energy spectrum (b) of daughter nuclei for the α -decay of ²⁴⁴Cm.

quadrupole deformations β_2 . If the β_2 value is increased from 0.200 to 0.230, minor changes in the b.r. to ground 0⁺ and excited 2⁺ states are seen. That is, the b.r. to ground 0⁺ states is decreased by 4.1% from its original value of 74.5% and the one belonging to excited 2⁺ states is increased by 4.2% from its original value of 25.3%. But the b.r. to excited 4⁺ and 6⁺ states have a strong dependence upon the β_2 value, as shown in figure 6(a). This is not so surprising because small components are of high sensitivity to internal factors in a complicated system, as stated above. Then, the effect of the excitation energy of daughter nuclei is examined. As the rotational band energy $E_I = \kappa_I I(I + 1)$ is changed from $E_2 = 40$ keV to $E_2 = 80$ keV, the b.r. to excited 2⁺ states is decreased by a factor of about 0.45 from its original value of 29.5%. Figure 6(b) illustrates the calculated b.r. to excited 4⁺ and 6⁺ states as a function of the excitation energy E_2 for the α -decay of ²⁴⁴Cm. One can see that such a decreasing trend becomes more significant as one proceeds to higher-spin states. This is due to the enhanced sensitivities and also because the excitation energies of the higher-spin states vary more obviously with κ_I than the low-lying states. The theoretical analysis presented above suggests that the b.r. to high-spin states constitute an important and sensitive probe of the structure properties of daughter nuclei. Recently, decay spectroscopy of heavy elements has been established and new high-statistics data have been obtained [40–45]. It would be of great interest to measure the α -decay intensity to high-spin states and explore the structure properties such as deformations and energy spectra.

The evolution of nuclear structure correlates with the integrated strength of the residual valence p - n interaction and the simple valence nucleon product $N_p N_n$ or $P = N_p N_n / (N_p + N_n)$ can be used to gauge this interaction [129]. Various structure quantities have been displayed to follow certain simple trends in the $N_p N_n$ scheme [130–135], such as nuclear deformation, $B(E2)$ values, ground band energies of even–even nuclei, core cluster decompositions in the rare earth region, yrast energies of even–even nuclei, α spectroscopic factors, and so on. Bucurescu and Zamfir also analyzed the α -decay fine structure of even–even nuclei in the P scheme [136, 137]. Three features were highlighted in terms of the

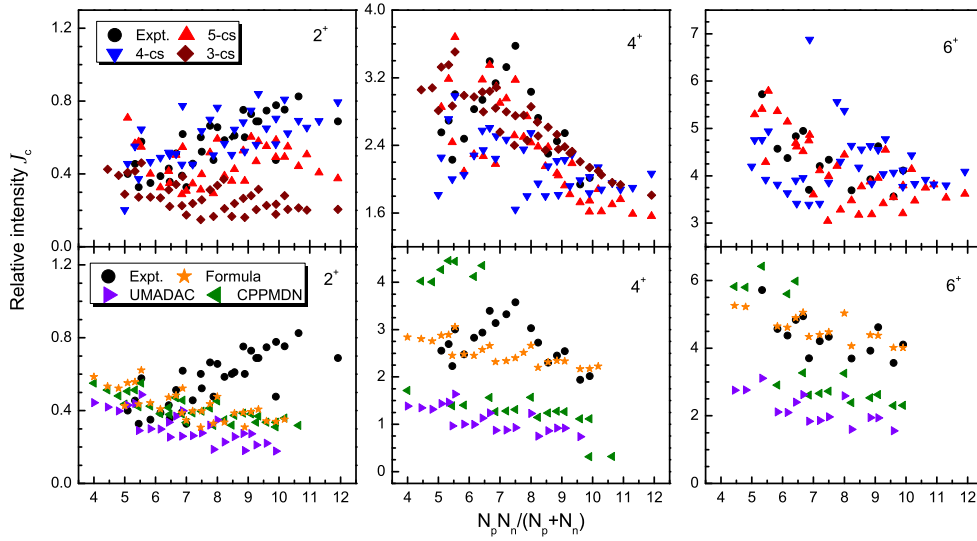


Figure 7. Relative intensities \mathcal{J}_c for excited $J = 2^+$, 4^+ , and 6^+ states as a function of the quantity $P = N_p N_n / (N_p + N_n)$ for well-deformed rotational daughter nuclei with $Z \geq 90$. Upper panel: the theoretical results are obtained using the coupled-channels approaches, containing the three-channels (3-cs) [59, 60], four-channels (4-cs) [57], and five-channels (5-cs) [58] calculations. Lower panel: the theoretical results are obtained using the semiclassical methods, containing the simple barrier penetration approach [86], the UMADAC [87], and the CPPMDN [89]. For the α -decay of ^{248}Fm , the \mathcal{J}_2 value obtained within the CPPMDN has a sudden increase by about two orders of magnitude with respect to the neighboring emitters [89], which is not displayed in the figure for the sake of clarity.

experimental data: (i) a practically exponential increase observed for excited 2^+ states for the collective nuclei (with $P \geq 4.0$); (ii) a marked maximum around $P \approx 7.5$ for excited 4^+ states; (iii) a decrease for excited 6^+ states, in the range $4.0 \leq P \leq 7.0$, a variation practically out of phase with that of the 4^+ state, after which there is a hint of stagnation or even slight increase. For even–even α -emitters, one also characterizes the α -decay fine structure by defining the relative intensity (2.28) [59, 60] which we rewrite here for convenience

$$\mathcal{J}_{J\ell} \equiv \log_{10}(\Gamma_{00}/\Gamma_{J\ell}), \quad (5.11)$$

where $\Gamma_{J\ell}$ represents the partial decay width of the channel (J, ℓ) . This quantity $\mathcal{J}_{J\ell}$ measures the relative intensity of different channels (J, ℓ) with respect to the favored channel $(0, 0)$. Figure 7 displays the calculated relative intensities $\mathcal{J}_{J\ell}$ for excited $J = 2^+$, 4^+ , and 6^+ states in the P scheme for well-deformed even–even rotational nuclei, compared with the systematics of the experimental data (the upper panel). The theoretical results contain the three-channels calculations of Delion *et al* [59, 60], the four-channels calculations with the diagonalization technique for the interaction matrix elements [57], and the five-channels calculations with the multipole expansion of the interaction potential [58]. For the case of excited 2^+ states, the four-channels and five-channels calculations show similarly good results and the three-channels analysis is slightly worse in the larger P region. For the case of excited 4^+ states, the results of the three cases appear to form a peak around $P \approx 7.5$ like the experimental results, but it is not evident especially in the smaller P region (corresponding to the outset of U, Pu, and Cm isotopic chains). This can be understood since in these α -decays,

members of negative-parity and excited-state rotational bands, such as $J = 1^-, 3^-, 0_2^+$, and 2_2^+ , emerge with low excitation energies in the daughter nuclei [46], leading to significant effects on the α -decay fine structure. The robust description of the fine structure observed in them requires suitable theoretical schemes to describe the coupling between different rotational bands. For the case of excited 6^+ states, the results of the four-channels and five-channels calculations follow the experimental points in both the systematic behavior and the magnitude, although the scattering of the theoretical points is relatively large. In particular, the five-channels results are able to explain the third experimental feature (iii) mentioned above. An obvious deviation from the experimental data is the four-channels result for the emitter ^{244}Pu . It should be further investigated. The coupled-channels calculations can give the results for excited 8^+ states as well, but there are quite few experimental data for the transitions to excited 8^+ states; that is, about six measurements are available [46], so they are not displayed in the figure. In addition, the semiclassical results for the fine structure were also analyzed in the P scheme, as shown in the lower panel of figure 7. The semiclassical calculations contain the simple WKB barrier penetration approach [86], the UMADAC [87], and the CPPMDN [89]. Within the CPPMDN, there is an abnormal point corresponding to the α -decay of ^{248}Fm where the calculated \mathcal{J}_2 -value has a sudden increase by about two orders of magnitude with respect to the neighboring emitters [89]. It is not displayed in the figure. The CPPMDN calculations for ^{248}Fm should be checked. As can be seen, the differences between the experimental data and the semiclassical results are much more considerable and the three main experimental features cannot be reproduced by them at all. This in turn gives an indirect support to the applicability and reliability of the coupled-channels approach.

Next, the multi-channel cluster model (MCCM) in the coupled channels framework was extended from even–even rotational nuclei to heavy odd-mass nuclei [109]. Instead of the α -decay to the g.s. rotational band, main attention is paid to the α -decay of odd-mass nuclei to the favored rotational band, which is quite similar to the α -decay of even–even nuclei to the g. s. rotational band. The number of decay channels one should consider increases greatly from even–even to odd-mass nuclei and varies from system to system. As it is known, enough channels are required for proper convergence in the numerical integration of the coupled equations. The coupled-channels studies for even–even nuclei suggest that the inclusion of all channels with $\ell \leq 6$ suffices for the description of the α -decay fine structure. For the sake of good convergence, all partial waves with $\ell \leq 8$ are used to decompose the total wave function for the α -decay of even–even rotational nuclei [58], where five channels are considered for one decay. According to the same rule, the number of decay channels for the α -decay to favored rotational bands depends on the spin-parity J^π of the parent state. This is because each member of the favored band exhibits several decay channels rather than a single channel. To be specific, the α -decays of ^{243}Cm and ^{255}Md from their ground states $5/2^+$ and $7/2^-$ to favored bands exhibit 21 and 24 decay channels, respectively. As a result, much effort was made to satisfy numerical requirements and much time was spent for numerical computation. Multi-channel calculations were performed for 32 deformed odd-mass emitters with $92 < Z < 103$ [109]. The calculated b.r. show good agreement with the available experimental data, within a factor of about 2.66. The detailed results can be found in tables (1–3) of [109]. It should be pointed out that for the α decay of ^{249}Cf from ground $9/2^-$ states, the b.r. to five low-lying members of the favored band are, respectively, known as 82.2(5)%, 4.69(5)%, 0.30(1)%, 0.0069%, and 0.00021% while the 25-channels calculations yield the values of 79.46%, 6.75%, 0.97%, 0.0117%, and 0.00221%. One can see that the largest deviation from the experimental data emerges at the transition from $9/2^-$ to $17/2^-$ by about one order of magnitude. But the recent high-resolution experiment [45] suggests the b.r. as 82.4(3)%,

Table 2. Comparison of the calculated b.r. with the experimental data for the α -transitions to seven low-lying members of the favored rotational band in the α -decay of ^{251}Cf and ^{253}Fm from their ground $1/2^+$ states. The b.r. is given as a percentage (in %). Calculations are performed within the MCCM and with the simple WKB barrier penetration approach. The calculated b.r. are normalized for comparison with the experimental data; that is, the sum of the calculated b.r. equals that of the experimental data.

Transition	E_I (keV)	b.r. (expt.)	b.r. (MCCM)	b.r. (WKB)
$^{251}\text{Cf} \rightarrow 1/2^+$	404.90(3)	35.4(5)	33.95	26.46
$\rightarrow 3/2^+$	433(2)	3.3(2)	4.24	9.13
$\rightarrow 5/2^+$	448(2)	4.9(2)	5.12	7.05
$\rightarrow 7/2^+$	516.68(11)	—	0.16	0.58
$\rightarrow 9/2^+$	550(2)	—	0.13	0.34
$\rightarrow 11/2^+$	652.5 ^a	—	0.00091	0.031
$^{253}\text{Fm} \rightarrow 1/2^+$	416.8(4)	23.2(9)	20.91	14.63
$\rightarrow 3/2^+$	440(4)	2.4(4)	3.15	5.90
$\rightarrow 5/2^+$	460(4)	2.6(5)	3.78	4.50
$\rightarrow 7/2^+$	514.1 ^a	—	0.19	1.84
$\rightarrow 9/2^+$	550.1 ^a	—	0.16	1.23
$\rightarrow 11/2^+$	635.2 ^a	—	0.0020	0.053
$\rightarrow 13/2^+$	687.2 ^a	—	0.0013	0.029

4.68(7)%, 0.29(1)%, 0.022(1)%, and 0.0022(3)%. The theoretical results are in excellent agreement with the new data. Besides, for the α -decay of even–even nuclei to the g.s. rotational band, one can notice that the b.r. to the member J is always larger than that to the higher-lying member ($J + 1$). This is consistent with the WKB barrier penetration formalism: as one proceeds to higher spin states, the decay energy decreases and the centrifugal barrier becomes higher, making the penetration even harder. However, in some cases concerning the α -decay of odd-mass nuclei to the favored rotational band, there is an inversion of b.r.. That is, the b.r. to excited ($I + 1$) states is larger than that to excited I states. Table 2 displays the calculated b.r. to seven low-lying members of the favored rotational band for the α -decay of ^{251}Cf and ^{253}Fm from their ground $1/2^+$ states. It is seen that the experimental b.r. to $5/2^+$ states is larger than that to $3/2^+$ states in both cases. The transition to $5/2^+$ states exhibits the same angular momentum $\ell = 2$ and the smaller decay energy with respect to the transition to $3/2^+$ states. In terms of the WKB barrier penetration approach, the b.r. to $5/2^+$ states should be smaller than that to $3/2^+$ states, as shown in table 2. This is in contradiction with the experimental data. By contrast, the MCCM results interpret well such an unexpected inversion and show good agreement with the data. For the α -transitions to the high-lying members such as $11/2^+$ and $13/2^+$ states, the experimental b.r. are still unknown and the differences between the MCCM and WKB results are considerable. Precise measurements of them would be most welcome to further test the validity and reliability of the two different approaches.

For comprehensiveness, the MCCM was also extended to heavy odd–odd nuclei [110]. Same as in the case of heavy odd-mass nuclei, one concentrated on the α -transitions to favored rotational bands, the remaining unpaired nucleons being unchanged. Owing to proton–neutron coupling on the one hand, the α -decay of well-deformed nuclei can take place not only from ground states but also from isomeric states; on the other hand, there are many complex rotational bands in daughter nuclei leading to some difficulties in measuring α -decay spectroscopy. Experimentally, spin-parities of daughter states cannot be assigned in many

cases and even spin-parities of parent states cannot be determined explicitly. Based on the NuDat database [46] and the Nubase2012 table [47], there are only four α -decays from ground or isomeric states available [46] for which the transitions to the low-lying members of the favored band have been observed. Furthermore, the spin-parities of the states involved in the transitions have been determined ambiguously or tentatively. In the calculations, enough decay channels are considered according to the same rule for even–even and odd-mass emitters. The number of the channels for odd–odd systems is comparable with the case of odd-mass nuclei and varies with the decaying state. For example, the α -decay of ^{240}Am from ground 3^- states to $K^\pi = 3^-$ rotational bands exhibits 23 decay channels and the α -decay of ^{242}Am from isomeric 5^- states to $K^\pi = 5^-$ rotational bands exhibits 25 decay channels. For comparison, the simple WKB barrier penetration approach was used to evaluate the b.r. to favored rotational bands as well. The details can be found in [110]. It is found that the WKB calculations seem to overestimate the b.r. to the second and third members of the favored band, while the MCCM calculations reproduce them well. This is quite similar to the calculations for even–even nuclei.

In the previous studies of odd-mass and odd–odd α emitters, main attention was paid to the α -decay to favored rotational bands, since in most cases such α -transitions play a dominant role in the fine structure. There are some special cases where the intensity to other rotational bands is non-negligible and even more significant as compared with the favored rotational band. Such special cases can be attributed to two aspects. One is that the favored rotational bands are located at the high excitation-energy region (>250 keV), so there are large differences between the decay energies to the favored band and to the low-lying band. This would enhance the influence of decay energy and hence reduce the dominant role of the favored band to some extent. The other is that some structure effects such as Coriolis mixing bring in the strong mixing of some low-lying states with the favored state. This would reduce the structure advantages of the favored band and hence the intensity to the favored band. The typical example is the α -decay of ^{249}Bk from the $7/2^+$ g.s. to four rotational bands in ^{245}Am . The new decay-spectroscopy experiment by Ahmad *et al* [44] suggests that the intensity to the g.s. rotational band $5/2^-$ [523] is as large as 96.816% while the intensity to the favored rotational band $7/2^+$ [633] is only about 2.8%. The similar feature is also seen in the α -decay of $^{243,245,247}\text{Bk}$, but it is less considerable [46]. Multi-channel calculations were further extended for the α -decay of odd-mass Bk isotopes from their ground states to more than one rotational band in the daughter Am nuclei [138]. The P_α factor reveals the structure differences between parent and daughter states, so it is expected to vary with different rotational bands in daughter nuclei for one α -decay. For the favored rotational bands, the P_α factor is fixed at $P_\alpha = 0.18$ for all the systems, which has been determined in the previous systematic calculations for heavy odd-mass nuclei [109]. Considering the astonishing similarity of the α decays from $^{243,245,247}\text{Bk}$, one can simply take the same preformation factor for one certain rotational band. That is, one obtains $P_\alpha = 0.0038$ for all the g.s. rotational bands $5/2^-$ [523] and $P_\alpha = 0.044$ for all the second rotational bands $5/2^+$ [642]. In the α decay of ^{249}Bk , the P_α factor is deduced as $P_\alpha = 0.034$ for the g.s. rotational band $5/2^+$ [642]. This P_α factor for the g.s. rotational band is significantly larger than in the cases of $^{243,245,247}\text{Bk}$. This confirms that there exists an admixture of the favored $7/2^+$ [633] state and the g.s. band in ^{245}Am . In the calculations, all the partial waves with $\ell \leq 8$ and with $\ell \leq 9$ are, respectively, considered for parity-unchanged and parity-changed transitions.

For the α -decay of $^{243,245,247}\text{Bk}$, the details can be found in table 1 of [138]. The calculated b.r. agree well with the available experimental data. The standard deviation of these calculations for 32 b.r. is evaluated as $\sigma = \{\sum_{i=1}^{32} [\log_{10}(\text{BR}_{\text{expt}}^i / \text{BR}_{\text{calc}}^i)]^2 / 31\}^{1/2} = 0.224$, which means that the α -decay fine

structures for these three Bk emitters is reproduced within a factor of about 1.67. For the α -decay of ^{249}Bk , the details can be found in figure 2 of [138]. The calculated b.r. by the MCCM show good agreement with the experimental data, generally within a factor of 2. In conclusion, the coupled-channels calculations of the MCCM give a robust and precise description of the α -transitions to the favored and unfavored rotational bands. Despite this, the correlation of final rotational bands is beyond the scope of the calculations, which requires suitable theoretical schemes. Efforts towards this are still needed.

6. Vibrational even–even nuclei

The so-called vibrational nuclei have zero or a small quadrupole deformation and the first excited 2^+ state has an energy of several hundreds of keV, i.e. much higher than for well deformed rotational nuclei. For this reason the α -transitions to higher states have practically vanishing decay widths.

The microscopic treatment of α -transitions to vibrational states in even–even nuclei within the Random Phase Approximation was given in [139–141]. Later on, the coupled channels analysis was performed in [142]. Here we summarize the main results. Let us consider an α -decay process $P \rightarrow D(J) + \alpha$, where J denotes the spin of the rotational state of an even–even nucleus, which in our case can be $J = 0, 2$. We describe the α -core dynamics by using the stationary Schrödinger equation (2.5) where the role of the core coordinate is played by the quadrupole vibrational collective coordinate $\xi_D = \alpha_2$. The Hamiltonian describing the α -decay is given by equation (2.6), where the interaction α -core potential is given by equation (2.23), i.e.

$$V(\mathbf{R}, \alpha_2) = \sum_{\lambda=0,2} \bar{V}_\lambda(R) \mathcal{Y}_\lambda(\Omega, \alpha_2), \quad (6.1)$$

with an angular part given by

$$\mathcal{Y}_0(\Omega, \alpha_2) = \frac{1}{\sqrt{4\pi}}, \quad \mathcal{Y}_2(\Omega, \alpha_2) = [Y_2(\Omega) \otimes \alpha_2]_0, \quad (6.2)$$

The monopole part of the interaction is given by the same ansatz as in equation (2.22). Concerning the $\lambda = 2$ formfactor, it is given by the linear term of the nuclear surface expansion, i.e.

$$\bar{V}_2(R) = -v_2(R - R_0) \frac{d\bar{V}_0(R)}{dR}. \quad (6.3)$$

The wave function is given similarly to the superposition (5.2), i.e.

$$\begin{aligned} \Psi(\mathbf{R}, \alpha_2) &= \frac{1}{R} \sum_{J=0,2} f_J(R) \mathcal{Z}_J(\Omega, \alpha_2) \\ \mathcal{Z}_J(\Omega, \alpha_2) &\equiv [Y_J(\Omega) \otimes \Phi_J]_0, \end{aligned} \quad (6.4)$$

where Φ_J is the J th eigenstate of the vibrational Hamiltonian $H_D(\alpha_2)$.

By using the orthonormality of angular functions entering the superposition (6.4), one obtains in a standard way the coupled system of differential equations for radial components (2.9), where the coupling matrix is given by (2.10). Only off diagonal matrix elements have non-vanishing values, given by

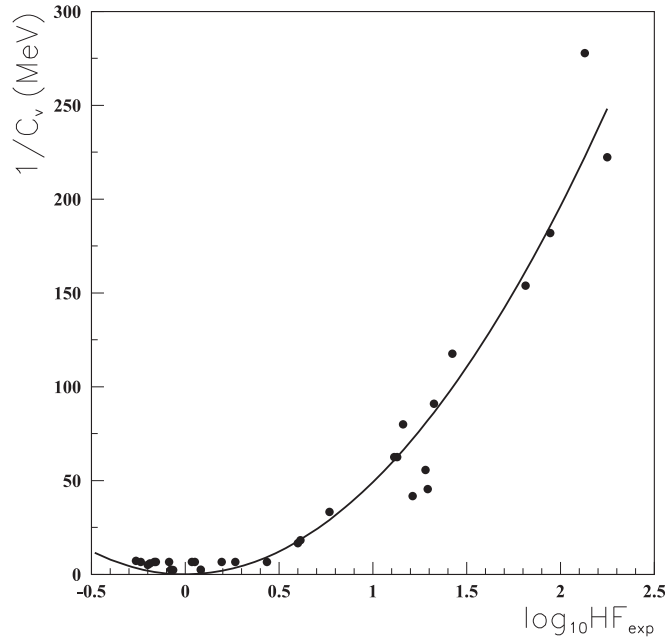


Figure 8. The inverse of the vibrational coupling parameter versus the logarithm of the experimental HF. The parabola is the fit given by (6.7). Adapted figure with permission from [142], Copyright (2007) by the American Physical Society.

$$\bar{V}_2(R) \langle \mathcal{Z}_2 | \mathcal{Y}_2 | \mathcal{Z}_0 \rangle = \frac{\bar{V}_2(R)}{\sqrt{4\pi}} \langle \Phi_2 | | \alpha_2 | | \Phi_0 \rangle \equiv -C_v (R - R_0) \frac{d\bar{V}_0(R)}{dR}, \quad (6.5)$$

and depending upon a new constant $C_v = v_2 \langle \Phi_2 | | \alpha_2 | | \Phi_0 \rangle / \sqrt{4\pi}$.

In [142], intensities and HFs for α -transitions to 2^+ states in even–even nuclei are investigated. The fine structure mainly depends upon the vibrational parameter C_v , defining the coupling strength between the two considered channels with $J = 0, 2$. Thus, in order to simplify the calculation, a value $v_a = 1$ was considered in equation (2.22), corresponding to a ‘pure’ α -cluster model. The α -decay fine structure was analyzed for those emitters with the known value of the intensity (2.28). Let us mention that the experimental data follows the rule (2.41), i.e.

$$\mathcal{J}_{\text{exp}} = 4.361 E_2 + 0.924, \quad \sigma = 0.774. \quad (6.6)$$

The calculations showed that this quantity can be reproduced for vibrational nuclei only by considering a strong repulsive core $c = 2000 \text{ MeV fm}^{-2}$, at variance with rotational emitters where it used a soft repulsion [59]. By using only one parameter C_v , it was possible to reproduce most of the experimental values \mathcal{J}_{exp} for vibrational emitters. The results of these calculations are given in table 1 of [142] for $Z = 76, \dots, 90$ even–even isotope chains. It is interesting to point out that the inverse of the vibrational coupling strength $1/C_v$ is proportional with the logarithm of the squared HF for all analyzed transitions, as it is shown in figure 8. Here the solid line represents the corresponding fit, i.e.

$$1/C_v = 49.122 (\log_{10} \text{HF})^2, \quad \sigma = 15.636. \quad (6.7)$$

In [142] it is shown that this relations allows one to predict the fine structure \mathcal{J} for several α -decays from vibrational nuclei by using the following relation

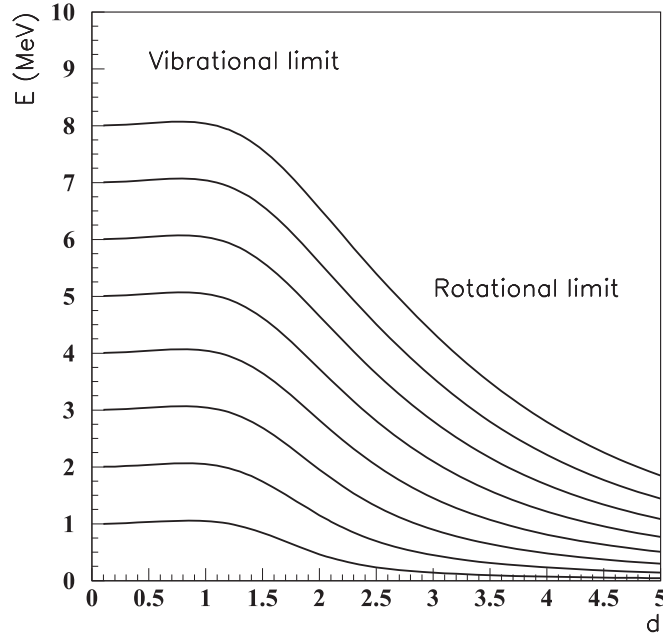


Figure 9. The expectation value of the harmonic Hamiltonian on the projected functions (8.2) versus the deformation parameter d .

$$\mathcal{J}_2 = 1/\sqrt{49.122 C_v} - \log_{10}(P_2/P_0). \quad (6.8)$$

The results for $Z = 76, 78, 80, 84, 86, 88, 90$ isotope chains are given in table 2 of [142].

7. Coherent state model (CSM)

The CSM was proposed in [143, 144] as a tool to describe in a unified way the spectra of vibrational, transitional and rotational nuclei. Within this model, the surface vibrations of a deformed nucleus are treated by using an exponential superposition of boson operators, describing the dynamics of the nuclear surface [145, 146]. The model was later extensively developed in [147, 148] for the description of low-lying as well as high spin states in nuclei, including isospin degrees of freedom (for a review, see [149]).

The ground state band in the even–even axially deformed daughter nucleus is given by the following ansatz

$$|\varphi_J^{(g)}\rangle = \mathcal{N}_J^{(g)}(d) \hat{P}_{M0}^J |e^{d(b_{20}^\dagger - b_{20})}|0\rangle, \quad (8.1)$$

where $\mathcal{N}_J^{(g)}$ denotes the normalisation, \hat{P}_{MK}^J is the standard angular momentum projection operator, $b_{2\mu}$ defines the boson operator describing surface oscillations and d is the CSM deformation parameter, proportional to the standard quadrupole deformation $d = \kappa\beta_2$ [150]. By changing this parameter it becomes possible to describe in an unified way vibrational, transitional and rotational spectra, as can be seen from figure 9, where we plotted the expectation value of the harmonic Hamiltonian on the projected functions (8.1)

$$E_J = \langle \varphi_j^{(g)} | \sum_{\mu} b_{2\mu}^{\dagger} b_{2\mu} | \varphi_j^{(g)} \rangle, \quad (8.2)$$

versus d . For an odd-mass nucleus, the state of total angular momentum I and projection M is projected from the product between the coherent state and a given spherical s.p. state ψ_j , where j is a shorthand notation for all of the quantum numbers of the state, that is

$$\Phi_{IM} = \mathcal{N}_{Ij}(d) P_{M0}^I[\psi_j e^{d(b_{20}^{\dagger} - b_{20})} |0\rangle] = \sum_J X_I^{Jj} [\varphi_j^{(g)} \otimes \psi_j]_{IM}, \quad (8.3)$$

where the amplitudes are given in [151].

7.1. Even–even emitters

Here we will summarize the results obtained in [150] and in the review [61] for even–even emitters. Let us consider an α -decay process connecting the g.s. to an excited level $P \rightarrow D(J) + \alpha$, where J denotes the spin of the state (8.1). Thus, the channel is defined by the spin $c = J$ and the core-angular harmonic is given by

$$\mathcal{Y}_J(b_2, \Omega) = [\varphi_j^{(g)}(b_2) \otimes Y_J(\Omega)]_0, \quad (8.4)$$

where $\mathbf{R} \equiv (R, \Omega)$ denotes the distance between the centers of the two fragments. The interaction potential between the α -particle and CSM core is described by the QQ ansatz (2.23), where the core quadrupole operator is given by

$$Q_{2\mu} = b_{2\mu}^{\dagger} + \tilde{b}_{2\mu} + a_{\alpha} [(b_2^{\dagger} \otimes b_2^{\dagger})_{2\mu} + (b_2 \otimes b_2)_{2\mu}]. \quad (8.5)$$

The matrix element of the α -core coupling entering equation (2.9) is proportional to the reduced matrix element of the QQ interaction [143]

$$\begin{aligned} & \langle \mathcal{Y}_J | V_d(b_2, \mathbf{R}) | \mathcal{Y}_{J'} \rangle \\ &= -C_0(R - R_{\min}) \frac{dV_0(R)}{dR} \frac{1}{\hat{2}\hat{J}\hat{J}'} \langle \varphi_j^{(g)} || Q_2 || \varphi_{j'}^{(g)} \rangle \langle Y_J || Y_2 || Y_{J'} \rangle \\ &= -C(R - R_{\min}) \frac{dV_0(R)}{dR} \frac{d}{\sqrt{4\pi}} \frac{\hat{J}}{\hat{J}'} \langle J0; 20 | J'0 \rangle^2 \left(\frac{\hat{J}' \mathcal{N}_j^{(g)}}{\hat{J} \mathcal{N}_{j'}^{(g)}} + \frac{\hat{J} \mathcal{N}_{j'}^{(g)}}{\hat{J}' \mathcal{N}_j^{(g)}} \right), \end{aligned} \quad (8.6)$$

Notice that the effective α -daughter coupling strength

$$C = C_0 \left(1 - \sqrt{\frac{2}{7}} a_{\alpha} d \right), \quad (8.7)$$

depends linearly on the deformation parameter.

In [61], an analysis of even–even emitters with known α -decay half-lives, fulfilling the vibrational/rotational condition within an error of 10% for the first four excited states was performed. First, the CSM deformation parameter d was determined by fitting four experimental energy levels E_J , for each nuclide where the data was available. The α -daughter coupling strength C defined by equation (8.7) was obtained from the reproduced values of the α -decay intensity \mathcal{J}_2 (2.28). The results are given in figure 10 as a function of the CSM deformation parameter. It is important to mention that the obvious linear correlation with a negative slope is predicted by the CSM model in equation (8.7). We also notice the strong correlation of the coupling strength with the reduced width, characterizing the α -clustering probability (proportional to the spectroscopic factor), also seen in figure 10.

The computed intensities \mathcal{J}_J (2.28) are given in [61], and the corresponding SFs (2.35) are shown in figure 11. Here we used the indices $i = 1, 2, 3$ to denote $J = 2, 4, 6$ states,

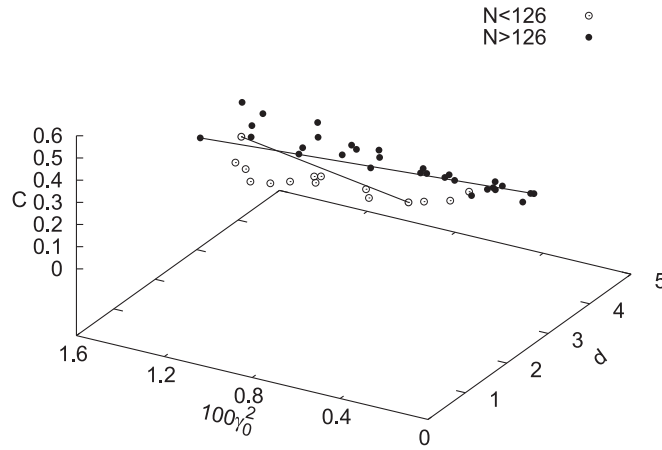


Figure 10. The α -core coupling strength versus the CSM deformation parameter and versus the reduced width multiplied by 100. The data are taken from [61].

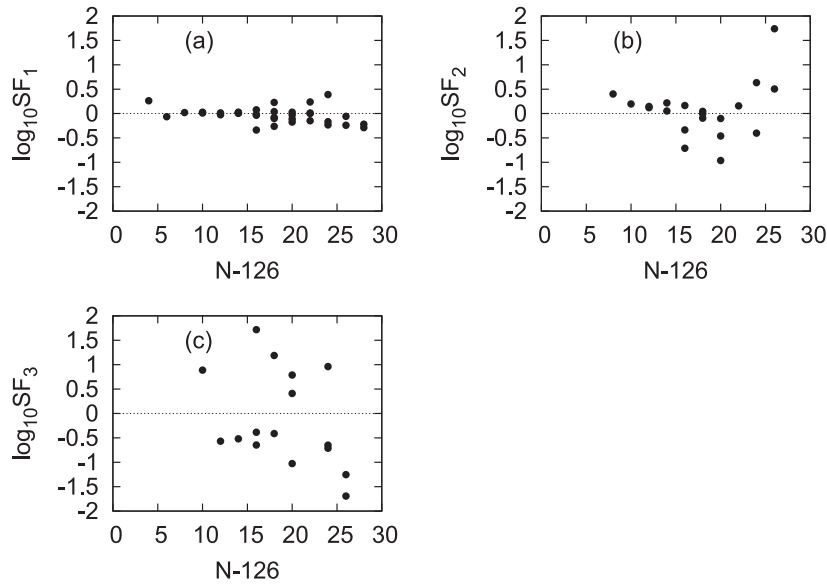


Figure 11. Panel (a) shows the logarithm of the suppression factor SF_1 for transitions to states with $J = 2$, versus the number labeling each nucleus. The same is true for panel (b) for $J = 4$ and panel (c) for $J = 6$.

respectively. The theoretical intensities were calculated by means of the linear dependence (8.7) between the α -daughter strength and deformation parameter d . The computed intensities for $J = 4$ are described within a factor less than 3, except Pu region. Let us mention that the logarithms of HFs, given by equation (2.30), have a similar behavior.

The α -decay spectrum is a very sensitive tool for the investigation of nuclear structure. Thus, the aforementioned maximum of the HF, or equivalently, the maximum of the intensity \mathcal{J}_J for the 4^+ state in the Pu region evidenced in [59] was recently related to the two-neutron separation energy, in connection to a deformed subshell corresponding to $N = 142$ [152]. This

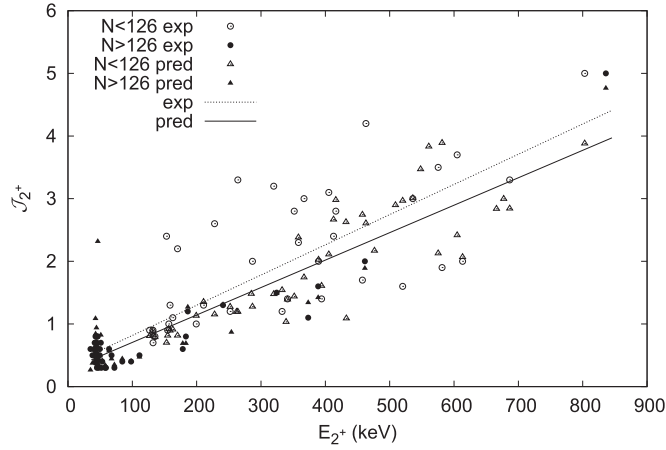


Figure 12. The intensity \mathcal{J}_2 versus the excitation energy E_2 of the daughter nucleus for experimental data and coupled channels results. The data are taken from [61].

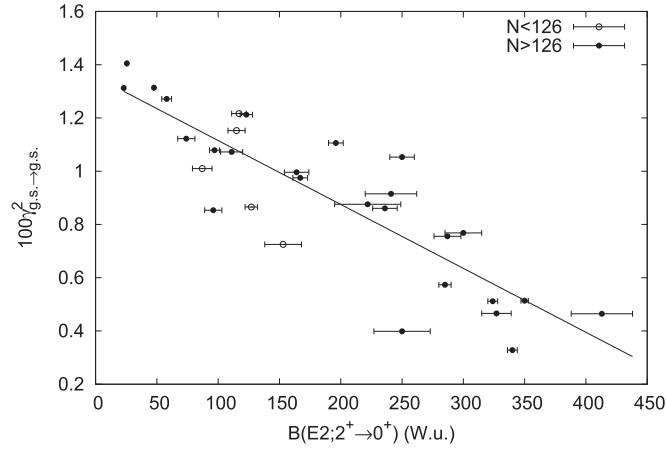


Figure 13. The reduced width multiplied by 100 versus the $B(E2)$ -values (all data is collected from [46]).

effect can be seen by representing the experimental values of \mathcal{J}_4 as a function of the Casten parameter $P = N_p N_n / (N_p + N_n)$ in [61].

Finally, in figure 12 we show the linear correlation between the intensity \mathcal{J}_2 and the excitation energy of the daughter nucleus E_2 predicted by equation (2.41) for all analyzed experimental data and the corresponding coupled channels results.

It is interesting to point out that the nuclear collectivity, given by reduced transition probability $B(E2; 2^+ \rightarrow 0^+)$, is closely related to the α -clustering, described by the reduced g.s. width γ_{gs}^2 defined by equation (2.17), as can be seen from figure 13. Therefore the largest α -clustering is characteristic for emitters above double magic nuclei with the smallest $B(E2)$ -values.

7.2. Favored odd-mass emitters

Several calculations for the fine structure of the emission spectrum for odd-mass α -emitters have already been analyzed in this review within the rotator model. We mention here [109], where a MCCM was used in conjunction with the coupled channels equation in order to calculate b.r. to excited states for favored transitions in heavy emitters, in the region $93 < Z < 102$. On the other hand, the unfavored g.s. \rightarrow g.s. α -decay in odd-mass nuclei in the region $64 \leq Z \leq 112$ was treated in [153], the main purpose being that of investigating the effect of the difference in the spin and parity of the ground states on the α -particle and daughter nucleus preformation probability. The calculations were done in the framework of the extended cluster model, with the WKB penetrability and assault frequency, together with an interaction potential computed on the basis of the Skyrme SLy4 interaction.

Here we will present the results of [151] concerning favored transitions in odd-mass α -emitters where the rotational band in which the parent decays is built on a spherical s.p. state of angular momentum projection $\Omega \neq \frac{1}{2}$. This band is described by equation (8.3) for an odd nucleon coupled to good angular momentum with a CSM core.

The decay phenomenon connects the g.s. of the parent nucleus of angular momentum I_P to an excited state of angular momentum I of the daughter and an α -particle of angular momentum ℓ

$$P(I_P) \rightarrow D(I) + \alpha(\ell). \quad (8.8)$$

The core-angular components are given by coupling the wave function of the odd-mass daughter nucleus to the spherical harmonic for the α -particle

$$\mathcal{Y}_{I\ell}(b_2^\dagger, \Omega) = [\Phi_I(b_2^\dagger) \otimes Y_\ell(\Omega)]_{I_P M_P}. \quad (8.9)$$

Each pair of angular momentum values defines a decay channel $(I, \ell) = c$. The coupling $Q_2.Y_2$ term of the matrix is found by the same method as in the previous section to be

$$\begin{aligned} \langle \mathcal{Y}_{I_1 \ell_1} | V_d(b_2^\dagger, \mathbf{R}) | \mathcal{Y}_{I_2 \ell_2} \rangle &= \sum_{J_1 J_2} X_{I_1}^{J_1} X_{I_2}^{J_2} \langle \varphi_{J_1}^{(g)} || Q_2^c || \varphi_{J_2}^{(g)} \rangle \langle \ell_1 || Y_2 || \ell_2 \rangle \\ &\times \hat{I}_P^2 \hat{I}_1 \hat{I}_2 \hat{j} (-)^{I_2 - I_P + \ell_2} W(I_1 I_1 I_2 \ell_2; I_P 2) \begin{Bmatrix} J_1 & I_1 & j \\ J_2 & I_2 & j \\ 2 & 2 & 0 \end{Bmatrix}, \end{aligned} \quad (8.10)$$

where the curly brackets denote a $9j$ -symbol. Since the reduced matrix element between the states of the core is a linear function of the deformation [148], one can still use an effective α -nucleus coupling strength given by equation (8.7).

The deformation parameter d was obtained by fitting available energy levels relative to the bandhead. The fitting formula agrees qualitatively with the similar treatment made for the ground bands of even-even nuclei in [61].

In the [151], the intensities

$$\begin{aligned} \mathcal{J}_i &= \sum_{\ell} \mathcal{J}_{I\ell} \\ \mathcal{J}_{I\ell} &= \log_{10} \frac{\Gamma_{\Omega 0}}{\Gamma_{I\ell}}, \end{aligned} \quad (8.11)$$

were investigated, where I was fixed by the angular momentum of the daughter nucleus in that particular state and ℓ followed from the triangle rule for the coupling to total angular momentum I_P . Here, the index $i \rightarrow I_{\text{head}} + i - 1$, where I_{head} corresponds to the bandhead spin.

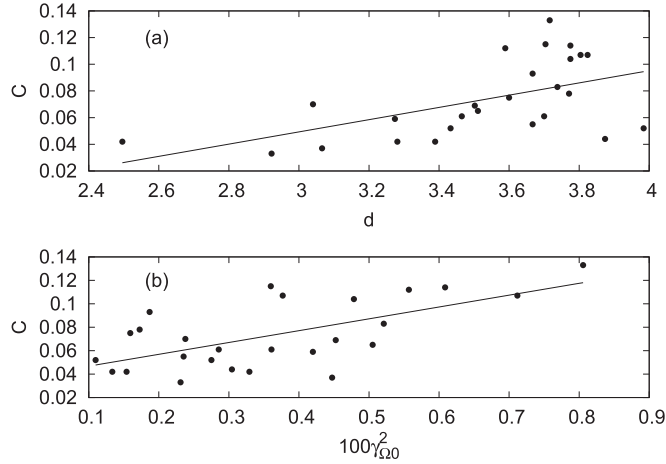


Figure 14. Panel (a) shows the effective α -nucleus coupling strength C versus deformation parameter d . Panel (b) presents the effective α -nucleus coupling strength C versus the reduced width $\gamma_{\Omega 0}^2$ for α -transitions to the bandhead. Adapted figure with permission from [151], Copyright (2016) by the American Physical Society.

It is sufficient to consider only one ℓ -value for each state. This is due to the fact that the standard penetrability P_{ℓ} through the Coulomb barrier, defined by the usual factorization (2.16) decreases by one order of magnitude for each increasing value of ℓ . Since the QQ interaction conserves parity, one must construct separate resonances of fixed even or odd parity. The even one follows the sequence of minimal ℓ -values in each channel as $\ell = 0, 2, 2, 4$, while the odd one follows the sequence $\ell = 1, 1, 3, 3$. Thus, each basis of four states having a given parity constructs a separate resonant solution of the system (2.9).

When plotted against the deformation parameter, the values of C obtained by fitting \mathcal{J}_1 values to experimental data, follow the prediction of equation (8.7) by exhibiting a linear trend with respect to d , as seen in figure 14 panel (a). This coupling strength can be interpreted as a measure of α -clustering because, as it turns out, C shows a linear correlation with $\gamma_{\Omega 0}^2$ with a positive slope, as can be seen in figure 14 panel (b).

In figure 15 we present in separate panels the values of the logarithms of the SFs defined by equation (2.35), obtained through the method presented above, versus the index number n found in the first column of table in [151]. It is clearly shown that coupling an α -particle to the daughter nucleus with the required strength needed to reproduce one value of the intensity (usually \mathcal{J}_1 , with the exception of Ac isotopes where \mathcal{J}_2 is reproduced) allows one to predict the values of the other intensities within a factor usually less than 3. We note that the universal decay law treated in [62] and [65] is once again observed in the dependence of the decay intensities on excitation energies. In figure 16, one notices the strong correlation between all of the \mathcal{J}_i values and the corresponding excitation energy E_i relative to the bandhead for each collective structure analyzed in [151].

8. Conclusions

We reviewed the status of the α -decay fine structure theoretical description especially within the coupled channels approach. The α -decaying states are identified as narrow outgoing resonances. The α -daughter potential is estimated within the double folding procedure of the

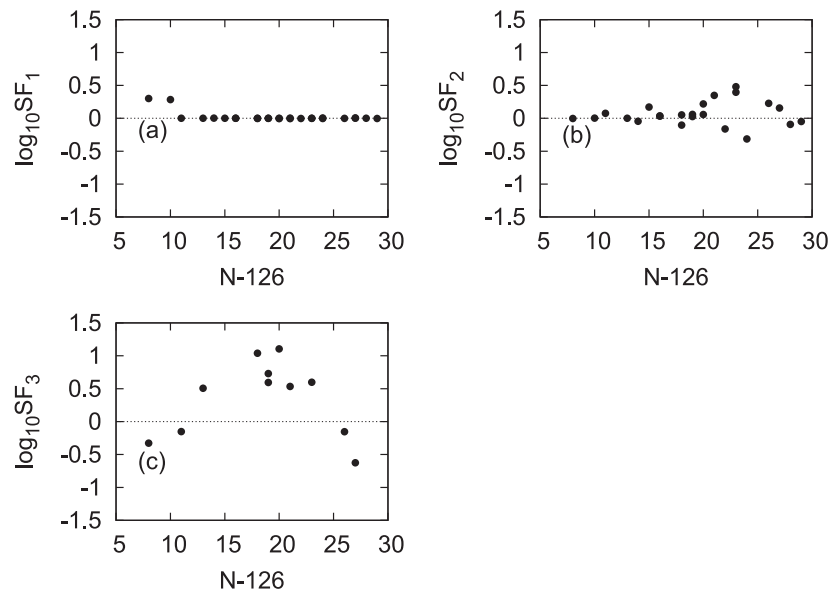


Figure 15. Logarithms of the suppression factors SF to the first three excited states in rotational bands as function of the index number n in the first column of table in [151]. Adapted figure with permission from [151], Copyright (2016) by the American Physical Society.

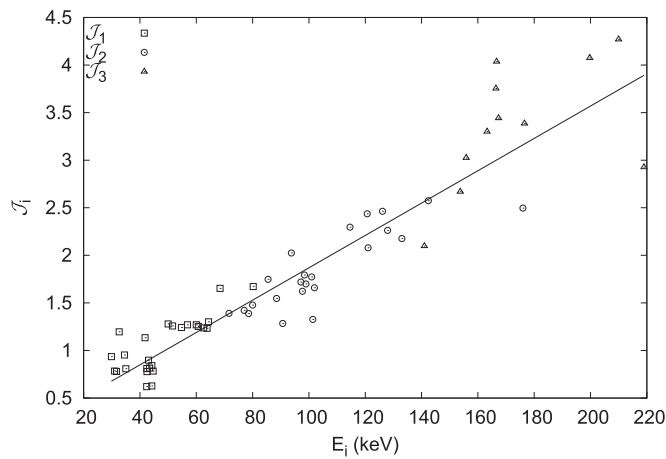


Figure 16. \mathcal{J}_i values versus excitation energy E_i relative to the bandhead in each case. Adapted figure with permission from [151], Copyright (2016) by the American Physical Society.

nuclear plus Coulomb nucleon–nucleon interaction. We described two equivalent methods to simulate the Pauli principle, which implies the existence of the α -particle on the nuclear surface, namely

- (i) the lowest narrow outgoing resonance in the pocket-like potential obtained by adding a repulsive core and
- (ii) the Wildermuth rule applied for states in the original double folding potential.

We analyzed transitions to rotational states described by the rigid rotator model, in even–even, odd–mass and odd–odd nuclei. The coupled-channels approach including enough decay channels gives a precise description of the α -decay fine structure observed in heavy deformed nuclei. The coupled-channels results are also compared with the semiclassical results. It is found that the semiclassical calculations overestimate the branching ratios (BR) to excited 4^+ states by about one order of magnitude for some even–even Pu, Cm, and Cf α -emitters and fail in explaining the unexpected inversion of branching ratios (i.e. $BR_{J+1} > BR_J$) in the α decay of some odd–mass nuclei, while the coupled-channels results show good agreement with the experimental data. Then we analyzed α -transitions to 2^+ vibrational states. Finally we have shown that the CSM is a powerful tool that can describe in a unified way vibrational, transitional and rotational nuclei. Our analysis evidenced several features of the α -decay fine structure

- (a) the linear dependence between α -intensities and excitation energy,
- (b) the linear correlation between the strength of the α -core interaction, reproducing fine structure, and spectroscopic factor, and
- (c) the inverse correlation between the nuclear collectivity, given by electromagnetic transitions, and α -clustering.

We conclude that the investigation of the α -decay fine structure is a very powerful tool to probe nuclear structure details. In particular, the α -decay intensity to high-spin states is closely correlated with the structure properties of daughter nuclei such as energy spectrum and deformation. Of course a major challenge for future is the microscopic description of unfavored α -transitions, where the structure of parent and daughter changes during the emission process.

Acknowledgments

This work was supported by the grants of Ministry of Research and Innovation (Romania), CNCS—UEFISCDI, project number PN-III-P4-ID-PCE-2016-0092, PN-III-P4-ID-PCE-2016-0792, within PNCDI III, and PN-18090101/2018, by the National Natural Science Foundation of China (Grants No. 11535004, 11035001, 11375086, 11105079, 10735010, 10975072, 11175085 and 11235001), and by the National Major State Basic Research and Development of China (Grant No. 2016YFE0129300), by the Science and Technology Development Fund of Macau under Grant No. 039/2013/A2.

ORCID iDs

D S Delion  <https://orcid.org/0000-0002-9982-0695>

References

- [1] Gamow G 1928 *Z. Phys.* **51** 204
- [2] Condon E U and Gurney R W 1928 *Nature* **122** 439
- [3] Lane A M and Thomas R G 1958 *Rev. Mod. Phys.* **30** 257

- [4] Mang H J 1960 *Phys. Rev.* **119** 1069
- [5] Săndulescu A 1962 *Nucl. Phys. A* **37** 332
- [6] Delion D S and Săndulescu A 2002 *J. Phys. G: Nucl. Part. Phys.* **28** 617
- [7] Delion D S, Săndulescu A and Greiner W 2004 *Phys. Rev. C* **69** 044318
- [8] Delion D S 2010 *Theory of Particle and Cluster Emission* (Berlin: Springer)
- [9] Segrè E 1964 *Nuclei and Particles: An Introduction to Nuclear and Subnuclear Physics* (New York: Benjamin)
- [10] Heyde K 1994 *Basic Ideas and Concepts in Nuclear Physics* (Bristol: IOP Publishing)
- [11] Rosenblum R 1929 *C. R. Acad. Sci. Paris* **188** 1401
- [12] Macfarlane R D and Griffioen R D 1963 *Phys. Rev.* **130** 4
- [13] Chu Y Y, Franz E M and Friedlander G 1968 *Phys. Rev.* **175** 1523
- [14] Coenen E, Deneffe K, Huyse M, Van Duppen P and Wood J L 1985 *Phys. Rev. Lett.* **54** 16
- [15] Toth K S, Wilmarth P A, Nitschke J M, Firestone R B, Vierinen K, Kortelahti M O and Avignone F T III 1988 *Phys. Rev. C* **38** 4
- [16] Liang C F, Paris P and Sheline R K 1994 *Phys. Rev. C* **49** 1872
- [17] Bijmens N *et al* 1995 *Phys. Rev. Lett.* **75** 25
- [18] Richards J D *et al* 1996 *Phys. Rev. C* **54** 4
- [19] Toth K S, Sousa D C, Batchelder J C, Nitschke J M and Wilmarth P A 1997 *Phys. Rev. C* **56** 6
- [20] Allatt R G *et al* 1998 *Phys. Rev. Lett.* **437** 29
- [21] Andreyev A N *et al* 1999 *Phys. Rev. Lett.* **82** 9
- [22] Page R D *et al* 1999 *J. Phys. G: Nucl. Part. Phys.* **25** 771
- [23] Kettunen H *et al* 2001 *Phys. Rev. C* **63** 044315
- [24] Liand C F, Paris P and Sheline R K 2001 *Phys. Rev. C* **64** 034310
- [25] Rudolph D, Baktash C, Devlin M, LaFosse D R, Riedinger L L, Sarantites D G and Yu C-H 2001 *Phys. Rev. Lett.* **86** 1450
- [26] Van de Vel K *et al* 2003 *Phys. Rev. C* **68** 054311
- [27] Andreyev A N *et al* 2004 *Phys. Rev. C* **69** 054308
- [28] Kettunen H *et al* 2004 *Phys. Rev. C* **69** 054323
- [29] Goldin L L, Novikova G I and Tretyakov E F 1956 *Phys. Rev.* **103** 4
- [30] Hollander J M, Smith W G and Rasmussen J O 1956 *Phys. Rev.* **102** 5
- [31] Bjørnholm S, Lederer M, Asaro F and Perlman I 1963 *Phys. Rev.* **130** 5
- [32] Dickens J K and McConnell J W 1980 *Phys. Rev. C* **22** 3
- [33] Ardisson G, Hussonnois M, LeDu J F, Trubert D and Lederer C M 1994 *Phys. Rev. C* **49** 6
- [34] Müller U, Sevenich P, Freitag K, Günther C, Herzog P, Jones G D, Kliem C, Manns J, Weber T, Will B and (ISOLDE Collaboration) 1997 *Phys. Rev. C* **55** 5
- [35] Hoellinger F *et al* 1999 *Phys. Rev. C* **60** 057301
- [36] Ardisson G, Gasparro J, Barci V and Sheline R K 2000 *Phys. Rev. C* **62** 064306
- [37] Ahmad I, Chasman R R, Greene J P, Kondev F G, Moore E F, Browne E, Porter C E and Felker L K 2003 *Phys. Rev. C* **68** 044306
- [38] Barci V, Ardisson G, Barci-Funel G, Weiss B, El Samad O and Sheline R K 2003 *Phys. Rev. C* **68** 034329
- [39] Rasmussen J O and Segal B 1956 *Phys. Rev.* **103** 1298
- [40] Herzberg R-D 2004 *J. Phys. G: Nucl. Part. Phys.* **30** R123
- [41] Lopez-Martens A *et al* 2011 *Nucl. Phys. A* **852** 15
- [42] Venhart M *et al* 2011 *Eur. Phys. J. A* **47** 20
- [43] Heßberger F P *et al* 2012 *Eur. Phys. J. A* **48** 75
- [44] Ahmad I, Greene J P, Kondev F G, Zhu S, Carpenter M P, Janssens R V F, Boll R A, Ezold J G, Van Cleve S M and Browne E 2013 *Phys. Rev. C* **87** 054328
- [45] Ahmad I, Greene J P, Kondev F G and Zhu S 2015 *Phys. Rev. C* **91** 044310
- [46] Evaluated Nuclear Structure Data Files of the Brookhaven National Laboratory (<http://nndc.bnl.gov/ensdf/>)
- [47] Audi G, Kondev F G, Wang M, Pfeiffer B, Sun X, Blachot J and MacCormick M 2012 *Chin. Phys. C* **36** 1157
- [48] Abele H and Staudt G 1993 *Phys. Rev. C* **47** 742
- [49] Khoa D T 2001 *Phys. Rev. C* **63** 034007
- [50] Neu R and Hoyle F 1992 *Phys. Rev. C* **46** 208
- [51] Avrigeanu M, Obreja A C, Roman F L, Avrigeanu V and von Oertzen W 2009 *At. Data Nucl. Data Tables* **95** 501

- [52] Mohr P, Kiss G G, Fülöp Z, Galaviz D, Gyürky Gy and Somorjai E 2013 *At. Data Nucl. Data Tables* **99** 651
- [53] Bertsch G, Borysowicz J, McManus H and Love W G 1977 *Nucl. Phys. A* **284** 399
- [54] Satchler G R and Love W G 1979 *Phys. Rep.* **55** 183
- [55] Cârstoiu F and Lombard R J 1992 *Ann. Phys. (NY)* **217** 279
- [56] Ni D D and Ren Z Z 2009 *Phys. Rev. C* **80** 051303(R)
Ni D D and Ren Z Z 2010 *Phys. Rev. C* **81** 024315
- [57] Ni D D and Ren Z Z 2010 *Phys. Rev. C* **81** 064318
- [58] Ni D D and Ren Z Z 2011 *Phys. Rev. C* **83** 067302
- [59] Delion D S, Peltonen S and Suhonen J 2006 *Phys. Rev. C* **73** 014315
- [60] Peltonen S, Delion D S and Suhonen J 2008 *Phys. Rev. C* **78** 034608
- [61] Delion D S and Dumitrescu A 2015 *At. Data Nucl. Data Tables* **101** 1
- [62] Delion D S 2009 *Phys. Rev. C* **80** 024310
- [63] Rasmussen J O 1959 *Phys. Rev.* **113** 1593
- [64] Viola V E and Seaborg G T 1966 *J. Inorg. Nucl. Chem.* **28** 741
- [65] Delion D S and Dumitrescu A 2015 *Phys. Rev. C* **92** 021303(R)
- [66] Ren Y J and Ren Z Z 2012 *Phys. Rev. C* **85** 044608
- [67] Delion D S, Liotta R J and Wyss R 2006 *Phys. Rev. Lett.* **96** 072501
- [68] Ni D D, Ren Z Z, Dong T K and Xu C 2008 *Phys. Rev. C* **78** 044310
- [69] Qi C, Xu F R, Liotta R J and Wyss R 2009 *Phys. Rev. Lett.* **103** 072501
- [70] Poenaru D N, Gherghescu R A and Greiner W 2012 *J. Phys. G: Nucl. Part. Phys.* **39** 015105
- [71] Parkhomenko A and Sobiczewski A 2005 *Acta Phys. Pol. B* **36** 3095
- [72] Blendowske R and Walliser H 1988 *Phys. Rev. Lett.* **61** 1930
- [73] Gurvitz S A and Kalbermann G 1987 *Phys. Rev. Lett.* **59** 262
- [74] Buck B, Merchant A C and Perez S M 1993 *At. Data Nucl. Data Tables* **54** 53
- [75] Xu C and Ren Z Z 2006 *Phys. Rev. C* **73** 041301(R)
Xu C and Ren Z Z 2006 *Phys. Rev. C* **74** 014304
- [76] Denisov V Y and Ikezoe H 2005 *Phys. Rev. C* **72** 064613
- [77] Chowdhury P R, Samanta C and Basu D N 2006 *Phys. Rev. C* **73** 014612
- [78] Kelkar N G and Castañeda H M 2007 *Phys. Rev. C* **76** 064605
- [79] Ismail M, Ellithi A Y, Botros M M and Abdurrahman A 2012 *Phys. Rev. C* **86** 044317
- [80] Poenaru D N, Ivascu M and Săndulescu A 1979 *J. Phys. G: Nucl. Phys.* **5** L169
- [81] Poenaru D N and Greiner W 1991 *Phys. Scr.* **44** 427
- [82] Gonçalves M and Duarte S B 1993 *Phys. Rev. C* **48** 2409
- [83] Royer G 2000 *J. Phys. G: Nucl. Part. Phys.* **26** 1149
- [84] Duarte S B, Tavares O A P, Guzmán F, Dimarco A, García F, Rodríguez O and Gonçalves M 2002 *At. Data Nucl. Data Tables* **80** 235
- [85] Xu C and Ren Z Z 2006 *Nucl. Phys. A* **778** 1
- [86] Zhang X, Xu C and Ren Z Z 2001 *Phys. Rev. C* **84** 044312
- [87] Denisov V Y and Khudenko A A 2009 *Phys. Rev. C* **80** 034603
Denisov V Y and Khudenko A A 2010 *Phys. Rev. C* **82** 059902
- [88] Wang Y Z, Dong J M, Peng B B and Zhang H F 2010 *Phys. Rev. C* **81** 067301
- [89] Santhosh K P, Sahadevan S and Joseph J G 2011 *Nucl. Phys. A* **850** 34
- [90] Delion D S, Patial M, Liotta R J and Wyss R 2016 *J. Phys. G: Nucl. Part. Phys.* **43** 095109
- [91] Akovali Y A 1998 *Nucl. Data Sheets* **84** 1
- [92] Fröman P O 1957 *Mat. Fys. Skr. Dan. Vid. Selsk.* **1** 3
- [93] Radi H M A, Shihab-Eldin A A, Rasmussen J O and Oliveira L F 1978 *Phys. Rev. Lett.* **41** 1444
- [94] Royer G 2010 *Nucl. Phys. A* **848** 279–91
- [95] Denisov V Y, Davidovskaya O I and Sedykh I Y 2015 *Phys. Rev. C* **92** 014602
- [96] Zhang S, Zhang Y, Cui J and Wang Y 2017 *Phys. Rev. C* **95** 014311
- [97] Buck B and Merchant A C 1989 *J. Phys. G: Nucl. Part. Phys.* **15** 615–35
- [98] Buck B and Merchant A C 1990 *J. Phys. G: Nucl. Part. Phys.* **16** L85–8
- [99] Buck B 1990 *Phys. Rev. Lett.* **65** 24
- [100] Buck B, Merchant A C and Perez S M 1991 *J. Phys. G: Nucl. Part. Phys.* **17** 1223–35
- [101] Buck B, Merchant A C and Perez S M 1991 *J. Phys. G: Nucl. Part. Phys.* **17** L91–4
- [102] Buck B, Merchant A C and Perez S M 1992 *J. Phys. G: Nucl. Part. Phys.* **18** 143–64
- [103] Buck B and Merchant A C 1992 *Phys. Rev. C* **45** 5
- [104] Buck B and Merchant A C 1993 *At. Data Nucl. Data Tables* **54** 53–73

- [105] Buck B 1994 *Phys. Rev. Lett.* **72** 9
- [106] Buck B and Johnston J C 1995 *Phys. Rev. C* **52** 4
- [107] Buck B 1995 *Phys. Rev. C* **51** 2
- [108] Buck B 1996 *Phys. Rev. C* **54** 4
- [109] Ni D D and Ren Z Z 2012 *Phys. Rev. C* **86** 054608
Ni D D and Ren Z Z 2012 *J. Phys. Conf. Ser.* **381** 012055
- [110] Ni D D and Ren Z Z 2013 *Phys. Rev. C* **87** 027602
- [111] Möller P and Nix J R 1995 *Nucl. Phys. A* **272** 502
- [112] Wildermuth K and Tang Y C 1997 *A Unified Theory of the Nucleus* (New York: Academic)
- [113] Hagino K, Rowley N and Kruppa A T 1999 *Comput. Phys. Comm.* **123** 143
- [114] Kruppa A T, Barmore B, Nazarewicz W and Vertse T 2000 *Phys. Rev. Lett.* **84** 4549
Barmore B, Kruppa A T, Nazarewicz W and Vertse T 2000 *Phys. Rev. C* **62** 054315
- [115] Suzuki Y and Ohkubo S 2010 *Phys. Rev. C* **82** 041303(R)
- [116] Ni D and Ren Z 2015 *Ann. Phys.* **358** 108
- [117] Lovas R G, Liotta R J, Insolia A, Varga K and Delion D S 1998 *Phys. Rep.* **294** 265
- [118] von Oertzen W, Feer M and Kanada-En'yo Y 2006 *Phys. Rep.* **432** 43 and references therein
- [119] Horiuchi H 2010 *J. Phys. G: Nucl. Part. Phys.* **37** 064021
- [120] Ohkubo S 1995 *Phys. Rev. Lett.* **74** 2176
- [121] Astier A, Petkov P, Porquet M-G, Delion D S and Schuck P 2010 *Phys. Rev. Lett.* **104** 042701
- [122] Fliessbach T, Mang H J and Rasmussen J O 1976 *Phys. Rev. C* **13** 1318
- [123] Tonzuka I and Arima A 1979 *Nucl. Phys. A* **323** 45
- [124] Varga K, Lovas R G and Liotta R J 1992 *Phys. Rev. Lett.* **69** 37
- [125] Hodgson P E and Běták E 2003 *Phys. Rep.* **374** 1
- [126] Xu C, Röpke G, Schuck P, Ren Z, Funaki Y, Horiuchi H, Tohsaki A, Yamada T and Zhou B 2017 *Phys. Rev. C* **95** 061306(R)
- [127] Stewart T L, Kermode M W, Beachey D J, Rowley N, Grant I S and Kruppa A T 1996 *Phys. Rev. Lett.* **77** 36
- [128] Einstein A 1917 *Phys. Z.* **18** 121
- [129] Casten R F 1985 *Phys. Rev. Lett.* **54** 1991
- [130] Casten R F and Zamfir N V 1993 *Phys. Rev. Lett.* **70** 402
- [131] Saha M and Sen S 1994 *Phys. Rev. C* **49** 2460
- [132] Buck B, Merchant A C and Perez S M 2005 *Phys. Rev. Lett.* **94** 202501
- [133] Ha E and Hong S W 2009 *Phys. Rev. C* **79** 037301
- [134] Ren Z and Xu G 1987 *Phys. Rev. C* **36** 456
Ren Z and Xu G 1988 *Phys. Rev. C* **38** 1078
- [135] Seif W M, Shalaby M and Alrakshy M F 2011 *Phys. Rev. C* **84** 064608
- [136] Bucurescu D and Zamfir N V 2012 *Rom. J. Phys.* **57** 69
- [137] Bucurescu D and Zamfir N V 2012 *Phys. Rev. C* **86** 067306
- [138] Ni D and Ren Z 2013 *Phys. Rev. C* **88** 014325
- [139] Delion D S and Liotta R J 1997 *Phys. Rev. C* **56** 1782
- [140] Delion D S and Suhonen J 2001 *Phys. Rev. C* **64** 064302
- [141] Peltonen S, Delion D S and Suhonen J 2005 *Phys. Rev. C* **71** 044315
- [142] Peltonen S, Delion D S and Suhonen J 2007 *Phys. Rev. C* **75** 054301
- [143] Raduta A A and Dreizler R M 1976 *Nucl. Phys. A* **258** 109
- [144] Raduta A A, Ceausescu V and Dreizler R M 1976 *Nucl. Phys. A* **272** 11
- [145] Lipas P O and Savolainen J 1969 *Nucl. Phys. A* **130** 77
- [146] Lipas P O, Haapakoski P and Honkaranta T 1976 *Phys. Scr.* **13** 339
- [147] Raduta A A, Ceausescu V, Gheorghe A and Dreizler R M 1981 *Phys. Lett. B* **99** 444
- [148] Raduta A A, Ceausescu V, Gheorghe A and Dreizler R M 1982 *Nucl. Phys. A* **381** 253
- [149] Raduta A A, Budaca R and Faessler A 2012 *Ann. Phys. (NY)* **327** 671
- [150] Delion D S and Dumitrescu A 2013 *Phys. Rev. C* **87** 044314
- [151] Dumitrescu A and Delion D S 2016 *Phys. Rev. C* **93** 024313
- [152] Bucurescu D and Zamfir N V 2013 *Phys. Rev. C* **87** 054324
- [153] Seif W M, Botros M M and Refaie A I 2015 *Phys. Rev. C* **92** 044302